Convergence and frequency-domain analysis of a discrete first-order model reference adaptive controller

Oreste S. Bursi[1,*,†,‡], D. P. Stoten[1,‡] and Leonardo Vulcan[2,§]

[1] *Department of Mechanical Engineering, University of Bristol, Bristol BS8 1TR, U.K.*
[2] *Department of Mechanical and Structural Engineering, University of Trento, 38050 Trento, Italy*

SUMMARY

We study the convergence properties of a direct model reference adaptive control system by applying techniques from numerical analysis. In particular, a first-order discrete system coupled to a minimal control synthesis algorithm discretized by the one-step one-stage zero-order-hold sampling is studied. This results in a strongly non-linear dynamic system owing to the adaptive mechanism where stability at steady state, i.e. at the operating point, equates to successful control. This paper focuses on the convergence analysis of the overall dynamical system for understanding accuracy, stability and performance at steady-state. The local stability of the steady state solution is considered by linearizing the system in the neighbourhood of an operating point when the input is a step function. This analysis allows us to specify two gain space domains which define the region of local stability. Moreover, both the accuracy and the frequency-domain analyses give insight into the range of adaptive control weightings that results in optimal performance of the minimal control synthesis algorithm and also highlights a possible approach to *a priori* selection of the time step and adaptive weighting values.

The effectiveness of the proposed analysis is further demonstrated by simulations and experiments on a first-order plant. Copyright © 2006 John Wiley & Sons, Ltd.

KEY WORDS: adaptive control; model reference; convergence analysis; local stability; frequency-domain analysis

1. INTRODUCTION

The use of adaptive control techniques has become a topic of increase interest in recent years as adaptive control can be used to control plants whose parameters are unknown or uncertain [1].

Adaptive control methods are generally divided into (i) direct and (ii) indirect methods. In the first case the adjustment rules provide directly how to update the controller parameters; in the indirect methods, the parameters of the unknown plant are estimated on-line, and the controller parameters are calculated on the base of these estimates. In the context of control theory some recent books and papers relevant to direct methods can be found [2,3]. In the context of structural control several applications have been made by several researches as well [4–6].

When a direct reference model controller is used, it can be also applied to systems where the details of the plant cannot be fully known *a priori* or are varying with time. Using this type of algorithms without the knowledge of plant parameters, such that we assume zero initial conditions for the controller gains, has become known as the minimal control synthesis (MCS) approach [7]. Basing adaptive control schemes on a reference model enables the system to be controlled to behave like the model itself. This type of approach [8,9] has been applied to a wide range of systems including non-linear and chaotic systems [3,10]. As the approach is based primarily on linear control theory being the reference model usually a linear one, the effect of non-linearities and/or disturbances in non-linear systems is compensated for by the adaptive nature of the controller. Very recently in the field of dynamic and seismic testing [11], the MCS method was used in real-time substructuring, in order to minimize the error between displacements imposed by the actuators on the substructure and displacements at the interfaces of the numerical model [12,13]; and it was adopted for seismic continuous pseudo-dynamic testing techniques [14].

Nowadays, controllers are implemented on digital computers, and therefore, the control systems must be directly written in digital form and/or transformed from continuous time to discrete time; moreover, if possible they must run in real-time and compensate for the influence of time delay [15]. As far as discretization methods are concerned, different one-step one/multi-stage real-time compatible algorithms are available, including the Euler method, the second- and the third-order Runge–Kutta methods [16], where in short, an integration method is defined to be real-time compatible, if the algorithm does not require the control signal $\mathbf{u}[k+1]$ at the time t_{k+1} to compute the plant response $\mathbf{x}[k+1]$. Also the zero-order-hold (ZOH) discrete equivalent is a one-step one-stage real-time compatible algorithm which provides exact result at sampling points for linear time invariant (LTI) systems and constant input in the time step [1, p. 42].

The selection of the best sample rate for a digital control system still represents a problem. Generally, the performance of a digital controller improves with increasing sampling rate, but costs may also increase with faster sampling; conversely, a slower sampling entails more time for control calculations and so slower computers with smaller word sizes and cheap A/D converters can be used. Thus generally, the slowest sample rate that meets all performance specifications is sought.

Though numerous studies have dealt with the stability and robustness properties of adaptive controllers [17,18], there is still a paucity of publications devoted to the clarification of specific computational issues, such as accuracy, stability, frequency behaviour, optimal choice of the sampling period and computational efficiency [19,20]. In detail, none of these aspects was considered yet for the MCS algorithm. All together, they represent basic aspects of the performance of the MCS algorithm and are the issues that the paper explores further by means of analyses, simulations and tests.

The remainder of the paper is organized as follows. In Section 2 the main characteristics of the basic MCS controller used in this paper are described. The relevant discrete control law and the parameters usually chosen for the controller are introduced in Section 3. In Section 4, the

local stability and accuracy analysis of the MCS controller is performed after the linearization of the overall dynamical system around an operating point, which corresponds to the steady state of the system. As the problem is particularly involved owing to the adaptation, conceptually simple linear first-order systems are considered for the plant, the reference model and the proof-of-concept tests. The properties of the MCS algorithm in the frequency domain are presented in Section 5. Then, the MCS algorithm is investigated by means of simulations and tests in Section 6. Finally, the main conclusions are presented in Section 7 along with comments on future work.

2. THE MINIMAL CONTROL SYNTHESIS ALGORITHM

This section introduces the MCS controller exploited in this study. This method is compared with a constant gain controller, developed assuming a linear system; conversely, the MCS is characterized by an adaptive portion, conceived to compensate for system non-linearities.

2.1. Constant gain controller and Erzberger's conditions

A generic non-linear plant can be described by the following equations:

$$\dot{\mathbf{x}}(t) = \mathbf{A}\mathbf{x}(t) + \mathbf{B}\mathbf{u}(t) + \mathbf{f}_{NL}(\mathbf{x}(t), t) \tag{1}$$

$$\mathbf{y}(t) = \mathbf{C}\mathbf{x}(t) \tag{2}$$

where $\mathbf{A}$ is the $n \times n$ matrix, $\mathbf{B}$ is the $n \times m$ input matrix, $\mathbf{x}(t)$ is the n-dimensional state vector, $\mathbf{u}(t)$ is the m-dimensional control input vector and $\mathbf{f}_{NL}(\mathbf{x}(t), t)$ represents the non-linear and time varying terms. $\mathbf{y}(t)$ and $\mathbf{C}$ are the output vector and plant output matrix, respectively, each having appropriate dimensions. A linear system with the same number of states, inputs and outputs is selected as reference model. The goal of the controller is for the dynamics of the actual non-linear system to match those of the reference model. The reference model has the following form:

$$\dot{\mathbf{x}}_m(t) = \mathbf{A}_m\mathbf{x}_m(t) + \mathbf{B}_m\mathbf{r}(t) \tag{3}$$

$$\mathbf{y}_m(t) = \mathbf{C}\mathbf{x}_m(t) \tag{4}$$

where $\mathbf{A}_m$ and $\mathbf{B}_m$ are $n \times n$ and $n \times m$ constant matrices, respectively, $\mathbf{x}_m(t)$ is the reference model state vector, $\mathbf{r}(t)$ is the m-dimensional reference input vector, and $\mathbf{y}_m(t)$ is the reference model output.

The error vector, $\mathbf{x}_e(t)$, can be defined as

$$\mathbf{x}_e(t) = \mathbf{x}_m(t) - \mathbf{x}(t) \tag{5}$$

The desired result is for the controller to drive the steady-state error, such that $\lim_{t \to +\infty} \mathbf{x}_e(t) = \mathbf{0}$ when this limit exists. Using the state feedback control, whose control law reads:

$$\mathbf{u}(t) = -\mathbf{K}\mathbf{x}(t) + \mathbf{K}_r\mathbf{r}(t) \tag{6}$$

By means of some mathematical manipulations, the error equation becomes:

$$\dot{\mathbf{x}}_e(t) = \mathbf{A}_m\mathbf{x}_e(t) + (\mathbf{A}_m - \mathbf{A} + \mathbf{B}\mathbf{K})\mathbf{x}(t) + (\mathbf{B}_m - \mathbf{B}\mathbf{K}_r)\mathbf{r}(t) - \mathbf{f}_{NL}(\mathbf{x}, t) \tag{7}$$

If

$$\mathbf{f}_{\mathrm{NL}}(\mathbf{x}, t) = \mathbf{0} \tag{8}$$

$$\mathbf{A}_m - \mathbf{A} + \mathbf{BK} = \mathbf{0} \tag{9}$$

$$\mathbf{B}_m - \mathbf{BK}_r = \mathbf{0} \tag{10}$$

are true, then (7) reduces to

$$\dot{\mathbf{x}}_e(t) = \mathbf{A}_m \mathbf{x}_e(t) \tag{11}$$

This ensures that $\mathbf{x}_e(t) \to \mathbf{0}$ as $t \to \infty$, as long as $\mathbf{A}_m$ is stable. Conditions (9) and (10) are used to determine the constant gains $\mathbf{K}$ and $\mathbf{K}_r$, i.e.

$$\mathbf{K} = \mathbf{B}^+(\mathbf{A} - \mathbf{A}_m)$$

$$\mathbf{K}_r = \mathbf{B}^+ \mathbf{B}_m \tag{12}$$

where the superscript plus sign ($^+$) denotes the pseudo-inverse: $\mathbf{B}^+ = (\mathbf{B}^{\mathrm{T}} \mathbf{B})^{-1} \mathbf{B}^{\mathrm{T}}$. It is assumed that $\mathbf{B}$ has full rank. If the Erzberger's conditions [21] for perfect model following are met, then $\mathbf{K}$ and $\mathbf{K}_r$ guarantee (9) and (10).

If Erzberger's conditions are not met, then the reference model needs to be redesigned. Nonetheless, if both the plant and the reference model have Luenberger-type controllable canonical structures, then Erzberger's conditions will be met [22].

2.2. Model reference adaptive controllers

When the plant is time varying or non-linear, then the $\mathbf{f}_{\mathrm{NL}}$ vector cannot be neglected. In order to compensate for the time-varying term, the model reference adaptive system (MRAS) theory introduces a time varying controller:

$$\mathbf{u}(t) = -(\mathbf{K} - \delta\mathbf{K}(t))\mathbf{x}(t) + (\mathbf{K}_r + \delta\mathbf{K}_r(t))\mathbf{r}(t) \tag{13}$$

where $\delta\mathbf{K}$ and $\delta\mathbf{K}_r$ are time varying gain adjustments. Substituting the control law (13) in (1) and after some manipulations, we get

$$\dot{\mathbf{x}}_e(t) = \mathbf{A}_m \mathbf{x}_e(t) + (\mathbf{A}_m - \mathbf{A} + \mathbf{BK})\mathbf{x}(t)$$
$$+ (\mathbf{B}_m - \mathbf{BK}_r)\mathbf{r}(t) - (\mathbf{B}(\delta\mathbf{K}_r\mathbf{r}(t) + \delta\mathbf{Kx}(t)) + \mathbf{f}_{\mathrm{NL}}(\mathbf{x},t)) \tag{14}$$

Again, $\mathbf{K}$ and $\mathbf{K}_r$ are selected so that the second and third terms in (14) are cancelled out. The error equation now reduces to

$$\dot{\mathbf{x}}_e(t) = \mathbf{A}_m \mathbf{x}_e(t) - \mathbf{B}(\delta\mathbf{K}_r\mathbf{r}(t) + \delta\mathbf{Kx}(t)) - \mathbf{f}_{\mathrm{NL}}(\mathbf{x},t) \tag{15}$$

The values of $\delta\mathbf{K}$ and $\delta\mathbf{K}_r$ must be selected to cancel the non-linear terms, but they cannot explicitly solved because $\mathbf{x}(t)$ is unknown. A stability proof for these controllers has been developed by using the hyperstability theory [22], which deals mainly with the stability of systems that can be broken into a linear feed-forward loop, which meets the strictly positive real condition, and a non-linear feedback loop that satisfies the Popov criterion for hyperstability. This problem is solved through the proper selection of the output error matrix $\mathbf{C}_e$, according to the Lyapunov problem.

Landau has presented a solution that yields expressions for $\delta\mathbf{K}$ and $\delta\mathbf{K}_r$ [22]:

$$\delta\mathbf{K}(t) = \int_0^t \boldsymbol{\varphi}_1(\tau)\,\mathrm{d}\tau + \boldsymbol{\varphi}_2(t)$$

$$\delta\mathbf{K}_r(t) = \int_0^t \boldsymbol{\psi}_1(\tau)\,\mathrm{d}\tau + \boldsymbol{\psi}_2(t) \tag{16}$$

A solution that satisfies the hyperstability condition for $\boldsymbol{\varphi}_1$, $\boldsymbol{\varphi}_2$, $\boldsymbol{\psi}_1$, and $\boldsymbol{\psi}_2$ is

$$\boldsymbol{\varphi}_1(\tau) = \alpha\mathbf{y}_e(\tau)\mathbf{x}^{\mathrm{T}}(\tau)$$

$$\boldsymbol{\varphi}_2(t) = \beta\mathbf{y}_e(t)\mathbf{x}^{\mathrm{T}}(t)$$

$$\boldsymbol{\psi}_1(\tau) = \alpha\mathbf{y}_e(\tau)\mathbf{r}^{\mathrm{T}}(\tau)$$

$$\boldsymbol{\psi}_2(t) = \beta\mathbf{y}_e(t)\mathbf{r}^{\mathrm{T}}(t) \tag{17}$$

where α and β are two positive constants, that must be selected before the solution of the above equations, and the output error $\mathbf{y}_e$ is

$$\mathbf{y}_e(t) = \mathbf{C}_e\mathbf{x}_e(t) \tag{18}$$

In order to ensure the stability of the closed loop system, $\mathbf{A}_m$ must have eigenvalues in the left-hand side of the complex plane. $\mathbf{A}_m$ should also have a Luenberger-type controllable canonical structure to ensure that Erzberger's conditions are satisfied.

The adaptive controller presented above requires the knowledge of the dynamic characteristics of the plant, $\mathbf{A}$ and $\mathbf{B}$, which allows evaluating the constant values of $\mathbf{K}$ and $\mathbf{K}_r$. This kind of drawback can be eliminated by using the MCS algorithm which derives from the MRAS formulation, but it assumes constant gains $\mathbf{K}$ and $\mathbf{K}_r$ equal to zero and unknown plant parameters [7]. Figure 1 shows the block diagram of a standard MCS controller with its essential components: the adaptive block; the input signal generation, $u(t)$; the plant; together with a parallel reference model; and a common reference signal, $r(t)$. The only elements that are needed to know are: the reference model parameters $\mathbf{A}_m$ and $\mathbf{B}_m$; the structure of the plant with the degree of freedom and order and the sign of the coefficients of $\mathbf{B}$, that usually is assumed positive. Therefore, the control law becomes

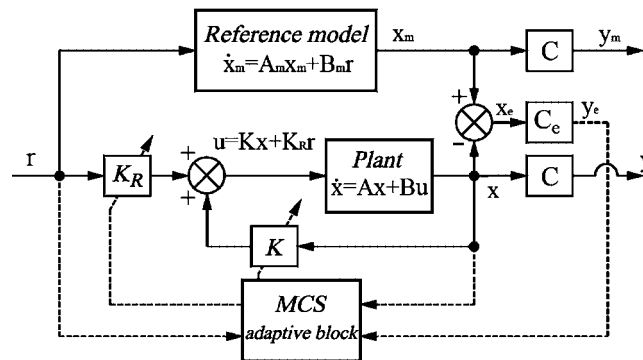$$\mathbf{u}(t) = \mathbf{K}(t)\mathbf{x}(t) + \mathbf{K}_r(t)\mathbf{r}(t) \tag{19}$$

Figure 1. Block diagram of the classical minimal control synthesis algorithm.

For the value of the output matrix $\mathbf{C}_e$, Stoten [9] proposed a pragmatic solution for first-order $\mathbf{C}_e = [4/t_s]$ and second-order $\mathbf{C}_e = [4/t_s \quad 1]$ one degree-of-freedom systems (DoFs), where t_s is the time settling of the system, that induces an exact pole-zero cancellation.

3. DISCRETE CONTROL LAW

Since usually the controller is digitally implemented, the continuous controller developed in the previous section must be discretized. This transformation is performed by the ZOH sampling process which exhibits several features among which, exact solution at sampling points for LTI systems and real-time compatibility. The discrete-time form of the reference model is defined by the mapping

$$\mathbf{x}_m[k+1] = \mathbf{\Phi}_m \mathbf{x}_m[k] + \mathbf{\Gamma}_m \mathbf{r}[k] \tag{20}$$

resulting in one-step one-stage method, where

$$\mathbf{\Phi}_m = e^{\Delta t \mathbf{A}_m} \quad \text{and} \quad \mathbf{\Gamma}_m = \int_0^{\Delta t} e^{\tau \mathbf{A}_m} \, d\tau \mathbf{B}_m \tag{21}$$

The sampling period or interval is $\Delta t = t_{k+1} - t_k$ and the discrete time variable is the integer k. The discrete control law equation for the MCS controller reads:

$$\mathbf{u}[k] = \mathbf{K}[k]\mathbf{x}[k] + \mathbf{K}_r[k]\mathbf{r}[k] \tag{22}$$

with the adaptive gains,

$$\mathbf{K}[k] = \mathbf{K}[k-1] + \beta \mathbf{y}_e[k]\mathbf{x}^{\mathrm{T}}[k] - \sigma \mathbf{y}_e[k-1]\mathbf{x}^{\mathrm{T}}[k-1] \tag{23}$$

$$\mathbf{K}_r[k] = \mathbf{K}_r[k-1] + \beta \mathbf{y}_e[k]\mathbf{r}^{\mathrm{T}}[k] - \sigma \mathbf{y}_e[k-1]\mathbf{r}^{\mathrm{T}}[k-1] \tag{24}$$

where $\sigma = \beta - \alpha \Delta t$ and the output error reads

$$\mathbf{y}_e[k] = \mathbf{C}_e \mathbf{x}_e[k] = \mathbf{C}_e(\mathbf{x}_m[k] - \mathbf{x}[k]) \tag{25}$$

Obviously, for the assumptions of the MCS algorithm, the initial conditions read

$$\mathbf{K}[-1] = \mathbf{0} \tag{26}$$

$$\mathbf{K}_r[-1] = \mathbf{0} \tag{27}$$

In order to complete the characterization of the MCS controller, the eigenvalues of the reference model, α and β from the adaptation equations, and $\mathbf{C}_e$ must be selected. The reference model must be stable, i.e. the eigenvalue moduli must be less than one, and should be selected so as not to exceed the system capability. The values of α and β are arbitrary positive numbers and are selected by trial and error. However, an increase of β means a reduction of the settling time of the adaptation, while a reduction of the β/α ratio improves the damping [21], Stoten proposed to set the ratio $\beta/\alpha = 0.1$. The final values of α and β are not critical, but they cannot be increased indefinitely because that may magnify noise within the loop. The selection of the error vector weighting matrix $\mathbf{C}_e$ is also relatively arbitrary and the selected values has been already introduced in the previous section for the continuous time system.

Due to the presence of the adaptive process, the MCS algorithm defines a non-linear dynamical system; then, for simplicity, we will consider first-order linear systems both for the plant and the reference model and we will perform the analysis on SDoF model equations assuming that the plant exhibits the fastest dynamics in the system. As a result:

$$x[k+1] = A'x[k] + B'u[k] \tag{28}$$

$$x_m[k+1] = A'_m x_m[k] + B'_m r[k] \tag{29}$$

where, owing to the ZOH sampling $A' = e^{-\Delta t/T}$, $B' = 1 - e^{-\Delta t/T}$, $A'_m = e^{-\Delta t/T_m}$, and $B'_m = 1 - e^{-\Delta t/T_m}$; T and T_m are, respectively, the plant and the reference model time constants; the low-frequency gain for the plant and the model are assumed equal to 1; and T_m is related to the approximate settling time t_s by $T_m = t_s/4$. Furthermore, the control signal and the reference input, that is assumed as a step function, read,

$$u[k] = K[k]x[k] + K_r[k]r[k] \tag{30}$$

$$r[k] = \begin{cases} 0, & k < 0 \\ 1, & k \geqslant 0 \end{cases} \tag{31}$$

respectively. In (30), we have implicitly assumed that the processing time δ is negligible with respect to Δt and therefore the control signal $u[k]$ generated by the MCS algorithm is obtained instantaneously and held constant over each time step. Furthermore,

$$y_e[k] = C_e x_e[k] \tag{32}$$

$$K[k] = K[k-1] + \beta y_e[k]x[k] - (\beta - \alpha\Delta t)y_e[k-1]x[k-1] \tag{33}$$

$$K_r[k] = K_r[k-1] + \beta y_e[k]r[k] - (\beta - \alpha\Delta t)y_e[k-1]r[k-1] \tag{34}$$

where $C_{e} = 4/t_s$ according to the pragmatic solution proposed in Reference [9].

4. STABILITY AND ACCURACY ANALYSIS

In this section, the innovative stability and consistency analyses of the MCS controller interpreted as a dynamical system are examined.

4.1. Amplification matrix and linearization

Combining Equations (28)–(30), (32)–(34) provides the multistep method

$$\begin{Bmatrix} x_e[k+1] \\ x[k+1] \\ K[k] \\ K_r[k] \end{Bmatrix} = \mathbf{A}_{IT} \begin{Bmatrix} x_e[k] \\ x[k] \\ K[k-1] \\ K_r[k-1] \end{Bmatrix} + \mathbf{B}_{IT} \begin{Bmatrix} x_e[k-1] \\ x[k-1] \\ K[k-2] \\ K_r[k-2] \end{Bmatrix} + \mathbf{g} \tag{35}$$

which can be interpreted as a second-degree iterative method [23, p. 486], where matrices $\mathbf{A}_{IT}$, $\mathbf{B}_{IT}$ and vector $\mathbf{g}$ are defined in Section A.1. This advancing scheme can be

expressed as

$$
\begin{Bmatrix}
x_e[k] \\
x[k] \\
K[k-1] \\
K_r[k-1] \\
x_e[k+1] \\
x[k+1] \\
K[k] \\
K_r[k]
\end{Bmatrix}
=
\begin{bmatrix}
\mathbf{0}_4 & \mathbf{I}_4 \\
\mathbf{B}_{IT} & \mathbf{A}_{IT}
\end{bmatrix}
\begin{Bmatrix}
x_e[k-1] \\
x[k-1] \\
K[k-2] \\
K_r[k-2] \\
x_e[k] \\
x[k] \\
K[k-1] \\
K_r[k-1]
\end{Bmatrix}
+
\begin{Bmatrix}
0 \\
0 \\
0 \\
0 \\
\mathbf{g}
\end{Bmatrix}
\tag{36}
$$

or

$$
\begin{Bmatrix}
x_e[k+1] \\
x_e[k] \\
x[k+1] \\
K[k] \\
K_r[k]
\end{Bmatrix}
= \mathbf{C}_{IT}
\begin{Bmatrix}
x_e[k] \\
x_e[k-1] \\
x[k] \\
K[k-1] \\
K_r[k-1]
\end{Bmatrix}
+
\begin{Bmatrix}
B_m' r[k] \\
0 \\
0 \\
0 \\
0
\end{Bmatrix}
\tag{37}
$$

where the amplification matrix $\mathbf{C}_{IT}$ is reported in Section A.1 too. The system is non-linear due to the presence of the adaptive mechanism; then, in order to reduce the complexity of the analysis, it will be locally developed by linearizing the system in a neighbourhood of an operating point, located at a steady-state condition for which $\lim_{x\to+\infty} x_e[k] \to 0$. The linearization by *physical insight* consists of simply substituting the values of the operating point, i.e. $x_e[k-1] = x_e[k] = 0$, $x[k-1] = x[k] = 1$ and $r[k-1] = r[k] = 1$ or a constant, in the amplification matrix $\mathbf{C}_{IT}$ defined in (A4). One can note that the system linearization could be obtained through a more rigorous linearization procedure based on a Taylor series expansion about the operating point [24, p. 657]. However, this procedure needs of the evaluation of the gains $K[k]$ and $K_r[k]$ at steady state which are unknown, consequently it can be performed only by means of preliminary numerical simulations [25]. For this reason the proposed analysis by *physical insight* is useful for *a priori* selection of the parameters and this will be proved by means of examples and tests illustrated in Section 6.

From (37) we get

$$
K_r[k] + K[k] = 1 \tag{38}
$$

where this relation of the Erzberger's gain must be considered valid at steady state [22]. It can be retrieved from (9) and (10) for first-order systems and implies that the ZOH sampling preserves this important property at discrete times. In this condition, (37) reads,

$$
\mathbf{y}[k+1] = \mathbf{C}_{IT,ss}\,\mathbf{y}[k] + \mathbf{l}[k] \tag{39}
$$

where

$$
\mathbf{C}_{IT,ss} =
\begin{bmatrix}
A'_m - 2B'\beta C_e & 2B'\sigma C_e & A'_m - A' & -B' & -B' \\
1 & 0 & 0 & 0 & 0 \\
2B'\beta C_e & -2B'\sigma C_e & A' & B' & B' \\
\beta C_e & -\sigma C_e & 0 & 1 & 0 \\
\beta C_e & -\sigma C_e & 0 & 0 & 1
\end{bmatrix}
\tag{40}
$$

$$
\mathbf{y}[k] =
\begin{Bmatrix}
x_e[k] \\
x_e[k-1] \\
x[k] \\
K[k-1] \\
K_r[k-1]
\end{Bmatrix}, \quad
\mathbf{l}[k] =
\begin{Bmatrix}
B'_m r[k] \\
0 \\
0 \\
0 \\
0
\end{Bmatrix}
\tag{41}
$$

As a result, the external stability of the MCS algorithm can be checked through the linearized matrix $\mathbf{C}_{IT,ss}$. For the subsequent analysis, it will be convenient to analyse the system in non-dimensional form by means of the following variables: $\Delta t/T_m$, $\beta/(4T_m)$, T/T_m, $\beta/(\alpha 4T_m)$.

4.2. External and equilibrium stability

Herein, first we perform the external stability analysis of the MCS controller, which is concerned with the boundedness of the response for bounded inputs [26]. In order to analyse this condition we recurrently apply (39) starting from the initial instant. We obtain:

$$
\mathbf{y}[k+1] = \mathbf{C}_{IT,ss}^{k+1}\mathbf{y}[0] + \sum_{j=0}^{k} \mathbf{C}_{IT,ss}^{k-j}\, \mathbf{l}[j]
\tag{42}
$$

Moreover, by using the spectral decomposition of matrices and vectors and considering (31), we obtain, if $\mathbf{C}_{IT,ss}$ is diagonalizable

$$
\mathbf{C}_{IT,ss} = \mathbf{\Phi}\mathbf{\Lambda}\mathbf{\Phi}^{-1}, \quad \mathbf{y}[0] = \mathbf{\Phi}\mathbf{c}, \quad \mathbf{l}[j] = \mathbf{\Phi}\mathbf{c}_f 1^j
\tag{43}
$$

where $\mathbf{\Phi}$, $\mathbf{\Lambda}$, $\mathbf{c}$ and $\mathbf{c}_f$ represent matrices of eigenvector and eigenvalues of $\mathbf{C}_{IT,ss}$, and vectors of the modal expansion of $\mathbf{y}[0]$ and $\mathbf{l}[j]$, respectively; thus, we end up with the modal expansions

$$
\mathbf{y}[k+1] = \mathbf{\Phi}\lambda^{k+1}\mathbf{c} + \sum_{j=0}^{k} \mathbf{\Phi}\lambda^{k-j}\mathbf{c}_f 1^j
$$

$$
= \sum_{s=1}^{5} \bar{\mathbf{c}}_s \lambda_s^{k+1} + \sum_{j=0}^{k}\sum_{s=1}^{5} \bar{\mathbf{c}}_{fs}\lambda_s^{k-j}
\tag{44}
$$

If all the eigenvalues of the matrix $\mathbf{C}_{IT,ss}$ are inside the unit circle and being the unit step input $\mathbf{l}[j]$ bounded, (42) is externally stable as shown in Section A.2. The expressions of λ_s are reported in the same subsection and they characterize the steady state error of the MCS algorithm. In detail, from the analysis of the eigenvectors with associated eigenvalues, $\lambda_1 = 1$ is a

characteristic of the MCS algorithm which indicates neutral stability and implies that the system gains wind up with noise due to presence of this eigenvalue [27]. Conversely, $\lambda_2 = 0$ corresponds to the condition of (38), which is referred to the absolute stability at steady state. While $\lambda_3 = e^{-\Delta t/T_m} < 1$ for $\Delta t > 0$, $\lambda_{4,5}$ can be real or complex conjugates, lower or greater than 1, such that the MCS algorithm may not be externally stable according to the combination of parameters.

If $\mathbf{l}[j] = \mathbf{0}$ in (42), the Lyapunov asymptotical and global stability can be studied analysing again the eigenvalues of $\mathbf{C}_{IT,ss}$. The MCS algorithm can be stable in the sense of Lyapunov, as the moduli of the eigenvalues of the matrix $\mathbf{C}_{IT,ss}$ are less than 1; this implies that initial and round-off errors do not artificially increase in the computation process. These stability notions are very important in order to assure that perturbations to the MCS scheme damp out during the computational process.
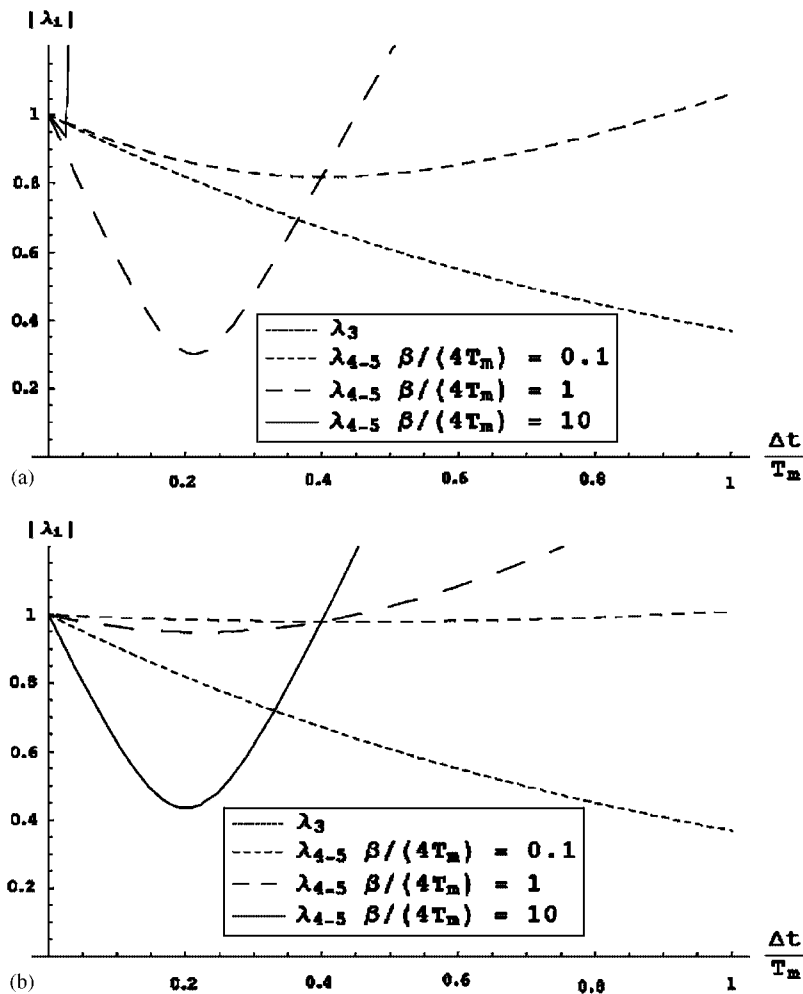

Figure 2. Eigenvalue moduli of the MCS controlled system for $\beta/(\alpha 4 T_m) = 0.1$ and a unit step input: (a) $T/T_m = 1$; and (b) $T/T_m = 10$.

The eigenvalues moduli of λ_3 and $\lambda_{4,5}$ for the unit step input (31) and two ratios of $T/T_m = 1$ and 10, are plotted in Figures 2(a) and (b), respectively. We assumed a time settling $t_s = 4T_m = 1$, $\beta/\alpha = 0.1$, as usually proposed for this algorithm, and, as a result, $\beta/(\alpha 4T_m) = 0.1$; while all remaining parameters can vary. Several observations can be made at this stage: (i) The MCS algorithm is only conditionally stable, as the eigenvalue moduli can exceed one, and the stability limit decreases for increasing values of $\beta/(4T_m)$; when $\lambda_{4,5}$ are complex conjugates such a limit is defined as

$$\left(\frac{\Delta t}{T_m}\right)_l = \frac{1}{2\alpha} + \frac{4}{\alpha}\frac{\beta}{4T_m} \qquad (45)$$

and does not depend on the T/T_m ratio, i.e. on the plant time constant. However, in practice the time step Δt is limited by the ratio $\left(\Delta t/T_m\right)_N = 0.5$, corresponding to the Nyquist frequency $1/(2\Delta t)$; and to accurately integrate the fastest component in the plant, one usually adopts $\left(\Delta t/T_m\right) = 0.1$ or a smaller ratio. (ii) The algorithmic damping provided by the MCS algorithm in order to reduce the error at steady state, i.e. for $k \gg 0$, increases with $\beta/(4T_m)$. (iii) The amount of damping introduced by the algorithm on (42) decreases for an increase of the T/T_m ratio. We must note that sometimes $\lambda_{4,5}$ become real and the stability limit reduces. This phenomenon is typical of time integration, for which in order to maximize the high-frequency dissipation, the principal roots shall remain complex conjugates as $\Delta t/T_m$ increases [28]. The values of $\beta/(4T_m)$ for which $\lambda_{4,5}$ become real are reported in Section A.2 and, as expected, these values depend on the plant characteristics. Rearranging (45), one can easily obtain the limit values of $\beta/(4T_m)$ as

$$\frac{\beta}{4T_m} = \frac{\beta/(\alpha 4T_m)}{2(\Delta t/T_m) - 8(\beta/\alpha 4T_m)} \qquad (46)$$

In the sampling interval–gain (SG) space represented in Figure 3 for $\beta/(\alpha 4T_m) = 0.1$ and a unit step input, (46) represents the stability limit of $\beta/(4T_m)$ as function of $\Delta t/T_m$ for complex $\lambda_{4,5}$ eigenvalues which, as stated before, does not depend on the T/T_m ratio, viz. on the plant. In this space the other bounds of the stability region are governed by the maximum modulus of λ_4–λ_5, which depend on the T/T_m ratio; these bounds for different T/T_m ratios are represented in Figure 3, too. Often in practice, the value $\Delta t/T_m = 0.1$ is chosen for accuracy reasons [29, p. 449], so the gain space (GS) domain depicted in Figure 4 represents the stability limit of $\beta/(4T_m)$ as function of the parameter $\beta/(\alpha 4T_m)$ with $\Delta t/T_m = 0.1$. Similar considerations can be made as there is a limit defined by complex eigenvalues independent of the plant. Again, the other bounds of the stability region are obtained when $\lambda_{4,5}$ are real for different values of T/T_m. Even in this plot, one can observe that the stability region increases with an increase of the T/T_m ratio. We can graphically see that the usual choice of assuming $\beta/(\alpha 4T_m) = 0.1$ is a good compromise between the adaptation mechanism speed and the stability limit, that is reduced for values smaller than 0.025 and it is not improved for values larger than 0.1. These stability domains may also be interpreted as an operational tool which allows the optimal combination of Δt–β/α values, which are usually set by trial and errors, even if the ratio T/T_m is unknown. The advantage of these spaces is that they permit to determine *a priori* substantial information on the behaviour of the sampled-data control system without knowing the plant.
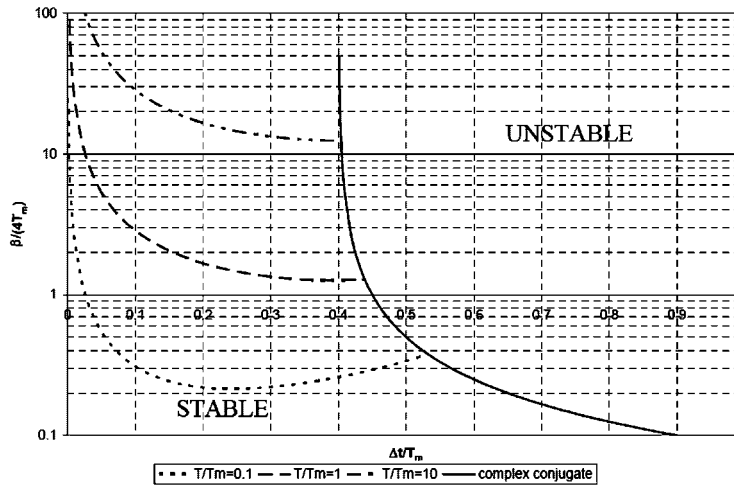
Figure 3. Asymptotic stability regions of the MCS algorithm in the sampling interval–gain space for a unit step input and $\beta/(\alpha 4 T_m) = 0.1$.
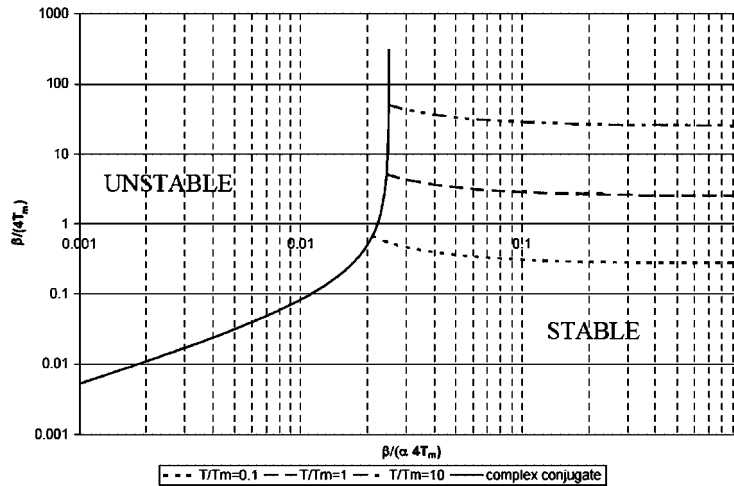

Figure 4. Asymptotic stability regions of the MCS algorithm in the gain space domain for a unit step input and $\Delta t / T_m = 0.1$.

In the foregoing stability analysis, we have not deliberately plotted λ_1 ($=1$) and λ_2 ($=0$), but only λ_3 and $\lambda_{4,5}$. Indeed, the response of the plant can be expressed as

$$x[k + 1] = \sum_{s=1}^{5} \bar{c}_{3s} \lambda_s^{k+1} + \sum_{j=0}^{k} \sum_{s=1}^{5} \bar{c}_{3fs} \lambda_s^{k-j} \tag{47}$$

and if we concentrate only on the first addendum of the right-hand side for equilibrium stability, we obtain that $\bar{c}_{31} = \bar{c}_{32} = 0$; therefore, only the remaining three coefficients and the
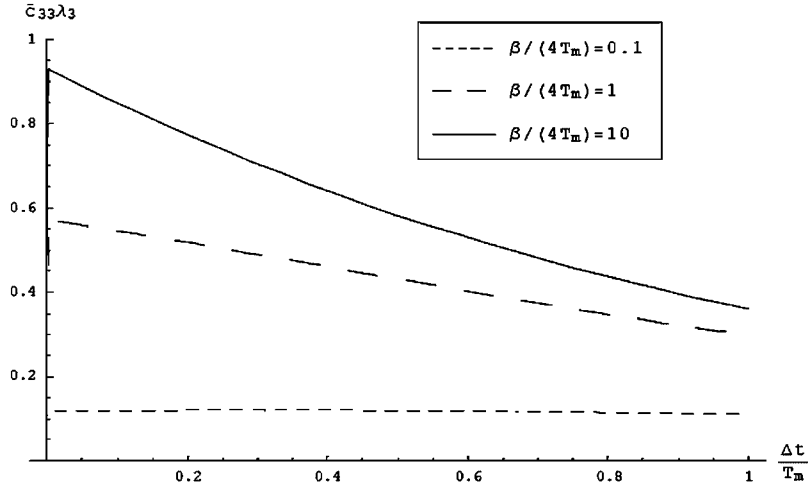
Figure 5. Evolution of $\bar{c}_{33}\lambda_3$ for $T/T_m = 10$, with a unit step input and $\beta/(\alpha 4 T_m) = 0.1$.

corresponding eigenvalues control the stability properties of the MCS controlled system. In this respect, Figure 5 shows the evolution of $\bar{c}_{33}\lambda_3$, which involves the real eigenvalue λ_3 as a function of $\Delta t/T_m$ for the unit step input and $T/T_m = 10$. One can observe that for the case considered, $\bar{c}_{33}\lambda_3$ is always less than 1 and the increase of $\bar{c}_{33}\lambda_3$ for increasing values of $\beta/(\alpha 4 T_m)$ is evident.

4.3. Accuracy

While for its definition a numerical algorithm is accurate when the computed numerical response approaches as much as desired the exact response, in the context of reference model controllers, we consider as exact the response of the reference model; at steady state as a result,

$$x_e[k] = x_m[k] - x[k] \quad \text{for} \quad k \gg 0 \tag{48}$$

will be interpreted as the error equation. Again, if we concentrate only on the first addendum of (44), the plant response can be expressed as

$$x[k+1] = \sum_{s=1}^{5} \bar{c}_{3s}\lambda_s^{k+1} = \exp(-\bar{\xi}\bar{\omega}\Delta t(k+1))(d_1 \cos(\bar{\omega}\Delta t(k+1))$$

$$+ d_2 \sin(\bar{\omega}\Delta t(k+1))) + \sum_{s=1}^{3} \bar{c}_{3s}\lambda_s^{k+1} \tag{49}$$

in which $\bar{\xi}$ defines the algorithmic damping ratio, $\bar{\omega}$ is the damped numerical frequency and d_i are constants determined from the initial conditions. For complex and conjugates eigenvalues, $\lambda_{4,5}$ can be represented as $C \pm iD$, then

$$\bar{\xi} = -\frac{\ln(C^2 + D^2)}{2\bar{\Omega}}, \bar{\Omega} = \arctan\left(\frac{D}{C}\right) \tag{50}$$

where $\bar{\Omega} = \bar{\omega}\Delta t$ is the non-dimensional damped numerical frequency.
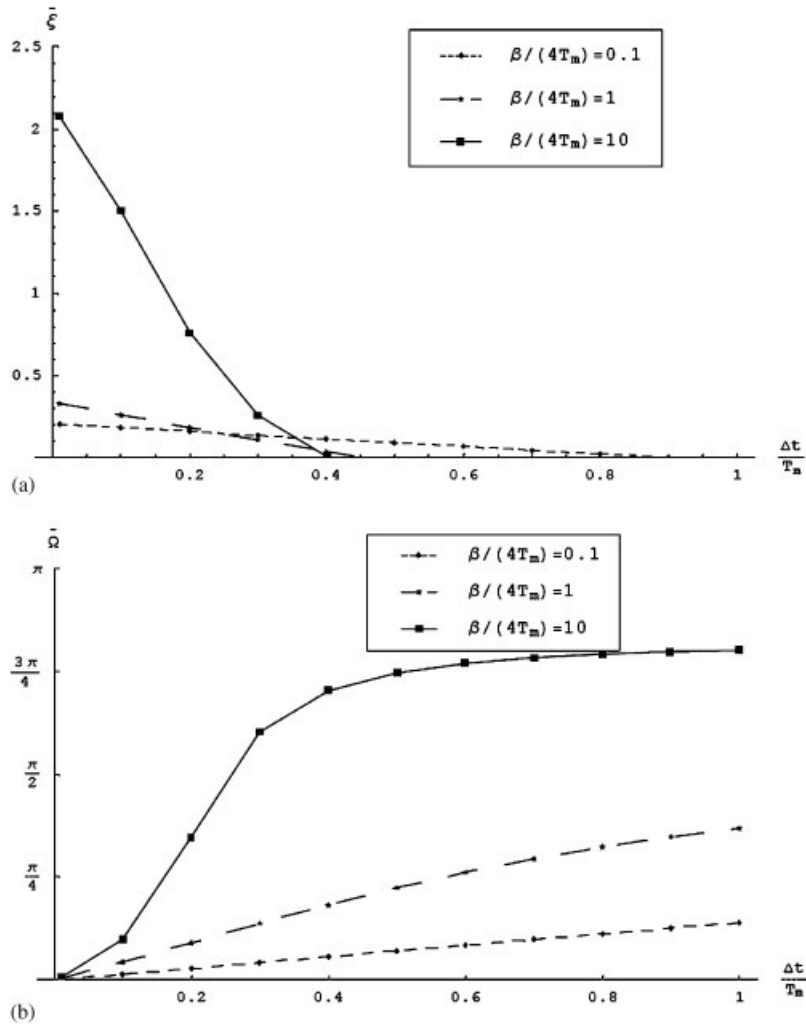
Figure 6. Algorithmic properties for $T/T_m = 10$ and unit step input: (a) damping ratio; and (b) non-dimensional damped natural frequency.

Both the algorithmic damping ratio and the damped frequency, which characterize the MCS algorithm, are represented in Figure 6 for $T/T_m = 10$ and unit step input. $\bar{\xi}$ clearly increases when $\beta/(4T_m)$ increases and $\Delta t/T_m$ reduces; conversely, $\bar{\xi}$ decreases when T/T_m increases. With regards to $\bar{\Omega}$, a clear increase of the numerical damped frequency with $\beta/(4T_m)$ is evident from Figure 6(b).

If we consider at steady-state, $x[k] = 1$ and (38), from the first two equations of (37) we get,

$$\left\{ \begin{array}{c} x_e[k+1] \\ x_e[k] \end{array} \right\} = \left[\begin{array}{cc} E_{11,\,ss} & E_{12,\,ss} \\ 1 & 0 \end{array} \right] \left\{ \begin{array}{c} x_e[k] \\ x_e[k-1] \end{array} \right\} = \mathbf{E}_{ss} \left\{ \begin{array}{c} x_e[k] \\ x_e[k-1] \end{array} \right\} \tag{51}$$

where

$$E_{11,\,ss} = \mathrm{e}^{-\Delta t/T_m} - 8\left(1 - \mathrm{e}^{-\Delta t/T}\right)\frac{\beta}{4T_m} \tag{52}$$

$$E_{12,\,ss} = 8\left(1 - \frac{\alpha\Delta t}{\beta}\right)\left(1 - \mathrm{e}^{-\Delta t/T}\right)\frac{\beta}{4T_m} \tag{53}$$

Analysing $E_{11,\,ss}$ and $E_{12,\,ss}$ we get,

$$E_{11,\,ss} = 1 \quad \text{for} \quad \frac{\Delta t}{T_m} \to 0; \quad E_{12,\,ss} = 0 \quad \text{for} \quad \frac{\Delta t}{T_m} \to 0 \tag{54}$$

A numerical integrator is defined as consistent if it reduces to zero the error between the numerical solution and the continuous-time solution when Δt approaches to zero. In the control context, (54) entails that, defining the error as difference between reference and plant states, the MCS algorithm is not consistent, as given two positive constants C_1 and p, $|x_e[k+1]| > C_1\Delta t^{p+1}$ with $p > 0$, where p is the so-called order of accuracy. In other words, the tracking error (48) does not vanish for $\Delta t \to 0$. This implies that the MCS algorithm discretized with the ZOH sampling is endowed with a global non-zero optimal sampling period $\Delta t/T_m$ which depends on $\beta/(4T_m)$. In this respect, the results of some numerical tests will be performed in the next subsection.

The spectral radius $\rho(\mathbf{E}_{ss}) = \rho_E$ is plotted in Figure 7 for unit step input, $T/T_m = 1$ and 10, respectively. First, one can observe that ρ_E can be greater than one and therefore, the MCS algorithm is only conditionally stable. Moreover, ρ_E does not vanish for $\Delta t/T_m \to 0$; in addition, an attentive reader can observe that below $\left(\Delta t/T_m\right)_N = 0.5$, ρ_E decreases for increasing values of $\beta/(4T_m)$.

4.4. Performance of the MCS algorithm

In order to validate the analysis of the previous subsection and to study the performance of the MCS algorithm we use a series of indicators in order to estimate the magnitude of the tracking error.

In detail to quantify the tracking error, we define the mean square tracking error,

$$X_e := \frac{1}{k_2 - k_1}\sum_{k=k_1}^{k_2} x_e^2[k] \quad \text{for } k_1\Delta t \geq t_s \tag{55}$$

and the tracking error bound

$$X_{e,\mathrm{sup}} := \sup|x_e[k]| \quad \text{for } k\Delta t \geq 2t_s \tag{56}$$

Relevant values provided by the application of the MCS algorithm are described in Figures 8–10, for different combinations of the parameters and $\beta/(\alpha 4T_m) = 0.1$. One may observe how the evolution of $|\lambda_{4,5}|$ of (40) with unit step input depicted in Figure 3 reflects well the amount of errors. This agreement can be also clearly observed in Figures 8(a) and (b), which report the tracking error bound $X_{e,\mathrm{sup}}$ for $T/T_m = 1$ and $T/T_m = 10$, respectively. As $X_{e,\mathrm{sup}}$ is defined at $t = 2t_s$ one can observe that also for this instant we have that the tracking error does not vanish for $\Delta t \to 0$, as predicted by (54). This trend is confirmed also for larger values of the time in which we have sampled the tracking error, as depicted in Figure 9. From this figure one
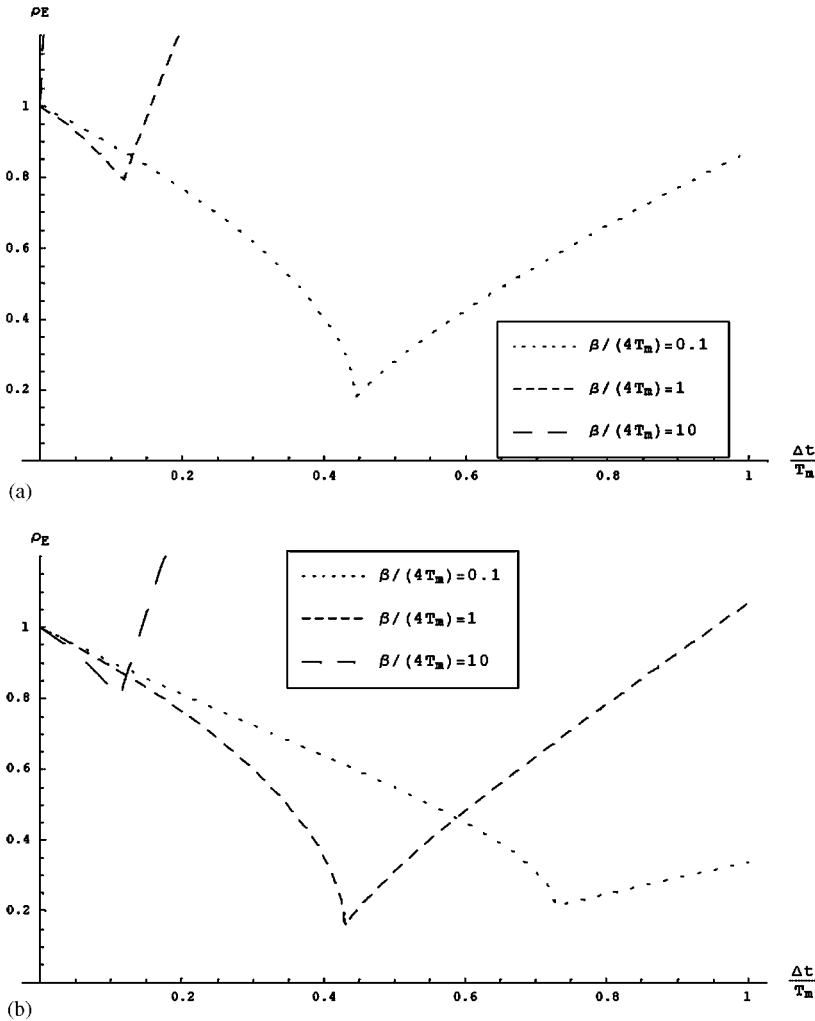
Figure 7. Spectral radius of $\mathbf{E}_{ss}$ for a unit step input: (a) $T/T_m = 1$; and (b) $T/T_m = 10$.

can see, that for small values of $\beta/(4T_m)$, the behaviour of $X_{e,\text{sup}}$ is more smooth at large $\Delta T/T_m$; this can be explained from (54) as $E_{11,ss}$ is closer to 1 for $\beta/(4T_m) = 0.1$. Figure 10 shows the mean square tracking error X_e defined in (55), assuming $k_2\Delta t = 2t_s$, for $T/T_m = 10$ and $r[k] = 1$. Similar considerations can be made as there is a correspondence between the tracking error and the spectral radius of the amplification matrix $\mathbf{C}_{IT,ss}$.

5. FREQUENCY-DOMAIN ANALYSIS

After the study of the MCS algorithm in the time domain, by means of convergence and stability analyses performed in Section 4, we turn our attention to frequency-domain analysis techniques.
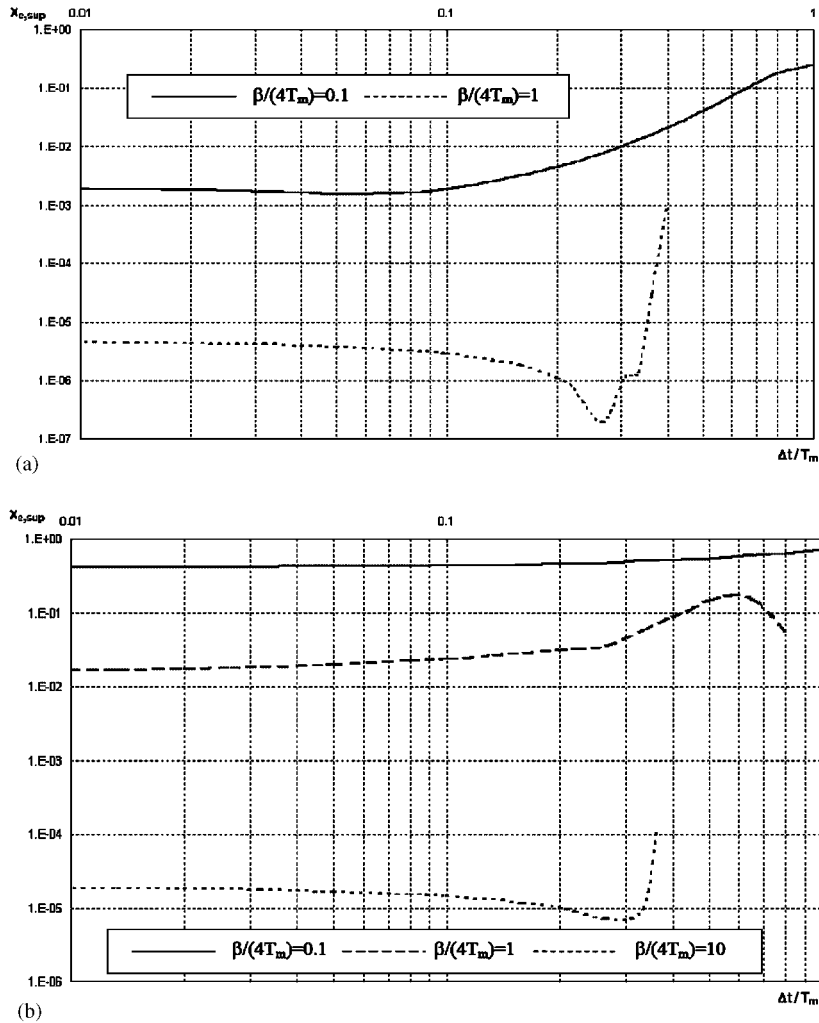
Figure 8. Convergence of $X_{e,\sup}$ for a unit step input: (a) $T/T_m = 1$; and (b) $T/T_m = 10$.

In fact, time domain analyses do not fully highlight the performance of a control algorithm; therefore we determine the steady-state response of the MCS algorithm to harmonic inputs in order to characterize its input–output behaviour. We will mainly follow techniques developed in Reference [30] for linear and non-linear systems.

5.1. Transfer and frequency response function vectors

Starting from the recurrence form of the MCS algorithm

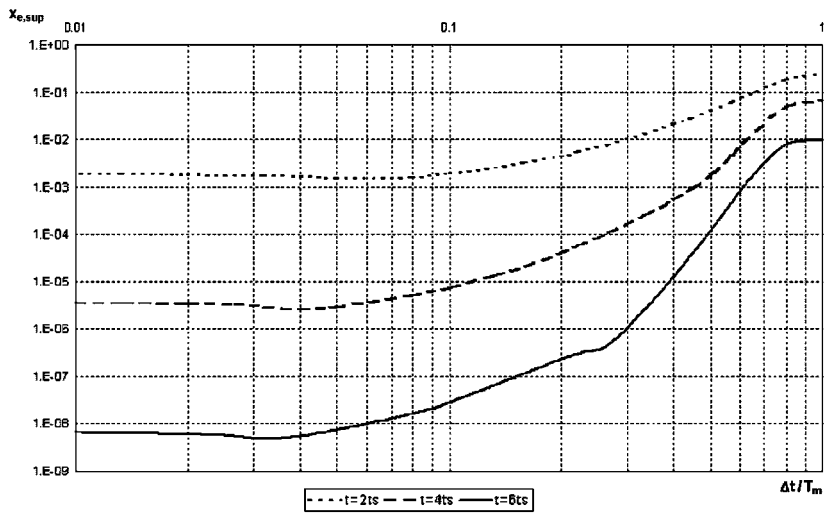$$\mathbf{y}[k + 1] = \mathbf{C}_{IT,ss}\mathbf{y}[k] + \mathbf{l}[k] \tag{57}$$

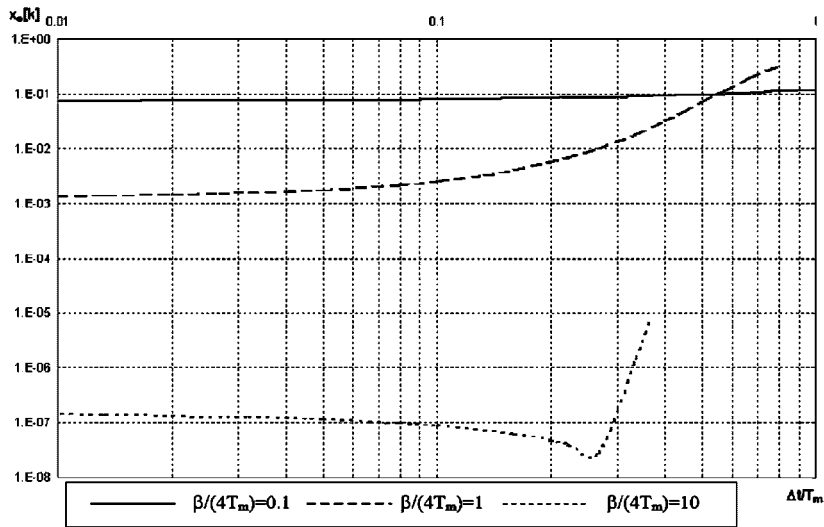Figure 9. Convergence of $X_{e,\,\mathrm{sup}}$ defined at different times t for $T/T_m = 1$ and a unit step input.

Figure 10. Convergence of X_e at $t = t_s$ for T/T_m and a unit step input.

and taking the one-sided z-transform (Z) of both sides of (57) one gets:

$$z\mathbf{Y}[z] - z\mathbf{Y}_0 = \mathbf{C}_{IT,\,ss}\mathbf{Y}[z] + B'_m[R[z], 0, 0, 0, 0]^{\mathrm{T}} \tag{58}$$

where $\mathbf{Y}[z] = Z[\mathbf{y}[k]]$ and $R[z] = Z[r[k]]$. Assuming zero initial conditions or that the transient part decays if the overall system is stable, (58) leads to the algorithmic transfer function vector:

$$\mathbf{G}[z] = \frac{\mathbf{Y}[z]}{R[z]} = (z\mathbf{I}_5 - \mathbf{C}_{IT,ss})^{-1} B'_m[1,0,0,0,0]^{\mathrm{T}} = [G_{x_{e1}}[z], G_{x_e}[z], G_x[z], G_K[z], G_{K_r}[z]]^{\mathrm{T}} \quad (59)$$

in which, for instance $G_x[z]$ relates the plant response and the input and can be interpreted as a receptance. Moreover, one can rewrite (59) as

$$\mathbf{G}[z] = \frac{\mathbf{Y}[z]}{R[z]} = \frac{\mathrm{adj}(z\mathbf{I}_5 - \mathbf{C}_{IT,ss})}{|z\mathbf{I}_5 - \mathbf{C}_{IT,ss}|} B'_m[1,0,0,0,0]^{\mathrm{T}} \quad (60)$$

where $\mathrm{adj}(^\circ)$ represents the adjoint operator and $|^\circ|$ the determinant. We observe that the poles of $\mathbf{G}[z]$ are equal to the roots of $|z\mathbf{I}_5 - \mathbf{C}_{IT,ss}|$, i.e. the eigenvalues of the $\mathbf{C}_{IT,ss}$ matrix. It is evident that external stability requires that the poles p_i of $\mathbf{C}_{IT,ss}$ are such that $|p_i| \leqslant 1$.

When the discrete demand is real and harmonic, i.e. $r[k] = \frac{1}{2}(R\mathrm{e}^{\mathrm{j}\tilde{\omega}k\Delta t} + R^*\mathrm{e}^{-\mathrm{j}\tilde{\omega}k\Delta t})$, the steady-state system response can be in turn assumed real and harmonic, i.e.

$$x[k] = \frac{1}{2}(X\mathrm{e}^{\mathrm{j}\tilde{\omega}k\Delta t} + X^*\mathrm{e}^{-\mathrm{j}\tilde{\omega}k\Delta t}) \quad (61)$$

where R, R^*, X and $X^* \in C$. Introducing such condition in (58), one obtains

$$\mathbf{G}[\mathrm{e}^{\mathrm{j}\tilde{\omega}\Delta t}] = [G_{x_{e1}}[\mathrm{e}^{\mathrm{j}\tilde{\omega}\Delta t}], G_{x_e}[\mathrm{e}^{\mathrm{j}\tilde{\omega}\Delta t}], G_x[\mathrm{e}^{\mathrm{j}\tilde{\omega}\Delta t}], G_K[\mathrm{e}^{\mathrm{j}\tilde{\omega}\Delta t}], G_{K_r}[\mathrm{e}^{\mathrm{j}\tilde{\omega}\Delta t}]]^{\mathrm{T}} \quad (62)$$

where $\mathbf{G}[\mathrm{e}^{\mathrm{j}\tilde{\omega}\Delta t}]$ is the vector of the algorithmic frequency response functions (AFRF) and $\tilde{\Omega} = \tilde{\omega}\Delta t$ is the non-dimensional angular frequency of the harmonic input demand $r[k]$. Some remarks have to be made at this point: (i) thanks to the form of $\mathbf{C}_{IT}$ in (A4), the linearization through *physical insight* does not require any assumption at steady state both of errors and of gains; (ii) as the Taylor series expansion of $r[k]$ is

$$r[k] = \frac{1}{2}\left(R\mathrm{e}^{\mathrm{j}\tilde{\omega}k\Delta t} + R^*\mathrm{e}^{-\mathrm{j}\tilde{\omega}k\Delta t}\right) = \frac{1}{2}(R + R^*) + \mathrm{j}\frac{1}{2}\left(R - R^*\right)\tilde{\omega}k\Delta t$$
$$- \frac{1}{4}(R + R^*)(\tilde{\omega}k\Delta t)^2 - j\frac{1}{12}(R - R^*)(\tilde{\omega}k\Delta t)^3 + O((\tilde{\omega}k\Delta t)^4) \quad (63)$$

and $R = R^*$ in this case, the evaluation of $r[k]$ in $\mathbf{C}_{IT,ss}$ defined in (40) is approximate as we are considering only the first term in the rhs of (63); (iii) consideration (ii) holds for $x[k]$ too; (iv) $\mathbf{G}[\mathrm{e}^{\mathrm{j}\tilde{\omega}\Delta t}]$ provides us information on the response of the sample data MCS controlled system when we select a single-frequency continuous time input $r[t] = \frac{1}{2}(R\mathrm{e}^{\mathrm{j}\tilde{\omega}t} + R^*\mathrm{e}^{-\mathrm{j}\tilde{\omega}t})$, sample $r[t]$ and apply $r[t]$ to the system. In this sense $\mathbf{G}[\mathrm{e}^{\mathrm{j}\tilde{\omega}\Delta t}]$ may be view as the AFRF of the sampled-data MCS algorithm.

5.2. Applications to the MCS algorithm

In order to characterize the behaviour of the MCS algorithm, we consider the following quantities $G_x[\mathrm{e}^{\mathrm{j}\tilde{\omega}\Delta t}]$ and $G_{x_e}[\mathrm{e}^{\mathrm{j}\tilde{\omega}\Delta t}]$ in terms of gain and phase Bode plots as a function of $\Delta t/T_m$ and $\tilde{\Omega}$. The algorithmic Bode gain plot of $G_x[\mathrm{e}^{\mathrm{j}\tilde{\omega}\Delta t}]$ is illustrated in Figure 11(a), while the phase, $\arg G_x[\mathrm{e}^{\mathrm{j}\tilde{\omega}\Delta t}]$, is illustrated in Figure 11(b), for $\beta/4T_m = 1$ and $T/T_m = 10$; the corresponding quantities for $\beta/4T_m = 10$ are reported in Figures 12(a) and (b), respectively. Several comments can be made on these representations. First, the response to a harmonic excitation (63) cannot be solved beyond the Nyquist frequency $\tilde{\Omega}_N = \tilde{\omega}_N\Delta t = \pi$ and this can be clearly observed both in Figures 11 and 12; moreover, we cannot have information on the annihilation capabilities of the MCS algorithm for $\Delta t/T_m \gg 0$, owing to the restriction of the Nyquist limit. Second, the
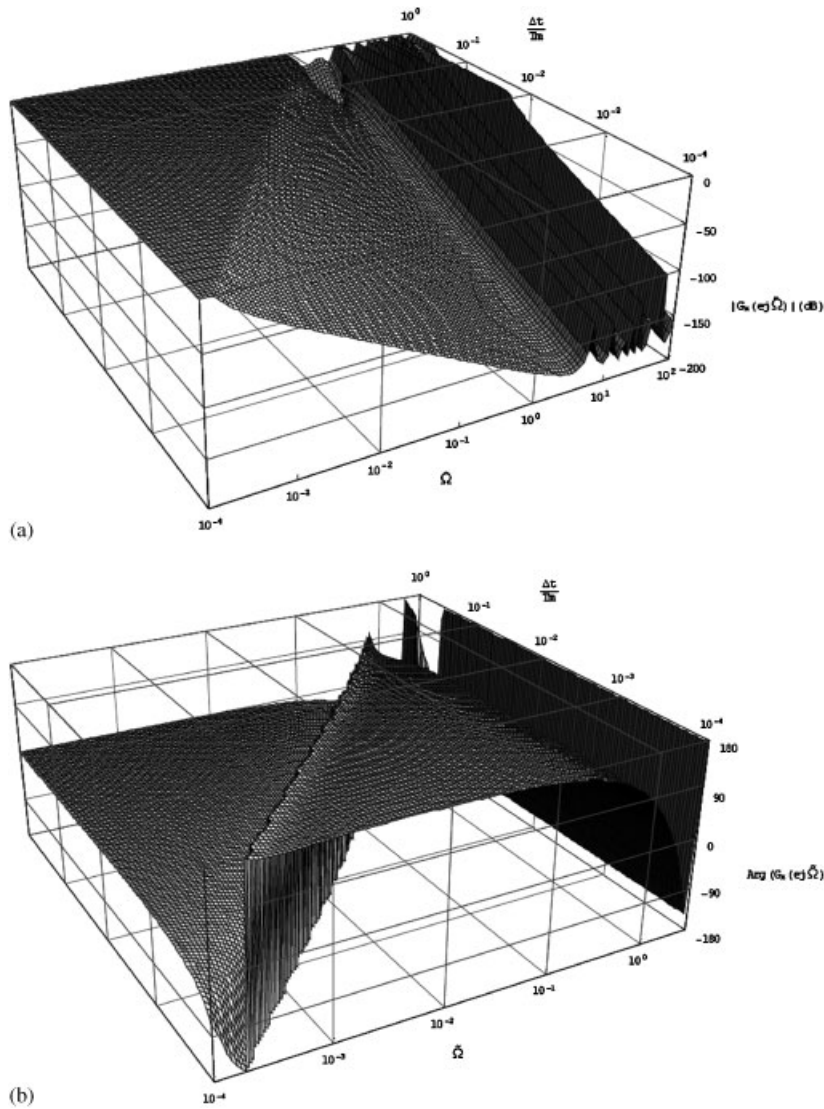
Figure 11. Plant response for $\beta/4T_m = 1$, $T/T_m = 10$ and unit step input: (a) gain Bode plot; and (b) phase Bode plot.

Bode magnitude decreases when $\tilde{\Omega}$ increases and it increases when $\Delta t/T_m$ increases; the first trend is wanted as high-frequency forcing components, for instance those caused by noise, can be damped out and this reflects the transfer function properties of the ZOH sampling [29, p. 155]; the second characteristic is unwanted as any integrated high-frequency component, for instance generated by the finite element method or due to stiff problem integration, present in the system is not attenuated when Δt is large or T_m is small. As far as the phase is concerned, we can observe from Figures 11(b) and 12(b) how it changes as a function of the $\beta/(4T_m)$ ratio;
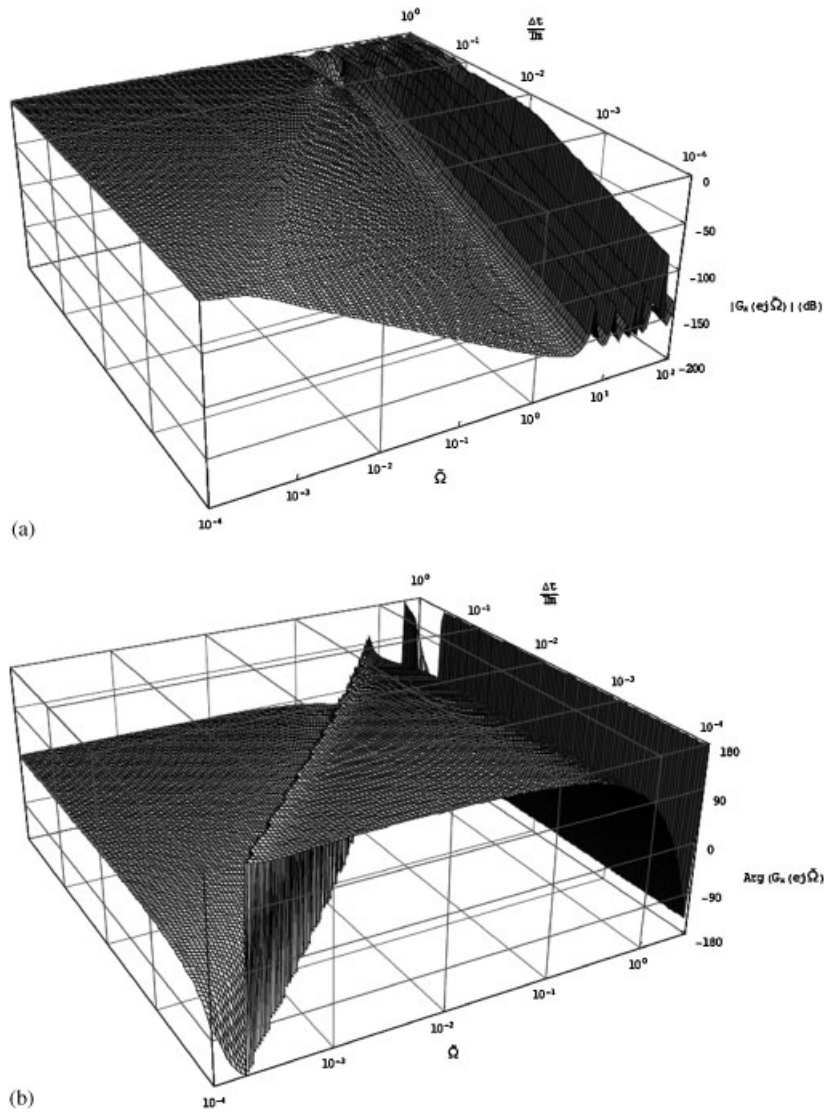
Figure 12. Plant response for $\beta/4T_m = 10$, $T/T_m = 10$ and unit step input: (a) gain Bode plot; and (b) phase Bode plot.

in addition the MCS algorithm changes from in-phase to out-of-phase with the forcing term as a function of $\tilde{\Omega}$.

The algorithmic gain Bode plot of $G_{x_e}[e^{j\tilde{\omega}\Delta t}]$, i.e. the transfer function of the tracking error, is illustrated in Figure 13(a), while the corresponding phase, arg $G_{x_e}[e^{j\tilde{\omega}\Delta t}]$, is depicted in Figure 13(b). One may observe that the gain does not reduce significantly for high values of $\tilde{\Omega}$; and in addition for very small values $\tilde{\Omega}$, the gain does not diminish for small values of $\Delta t/T_m$. Again,
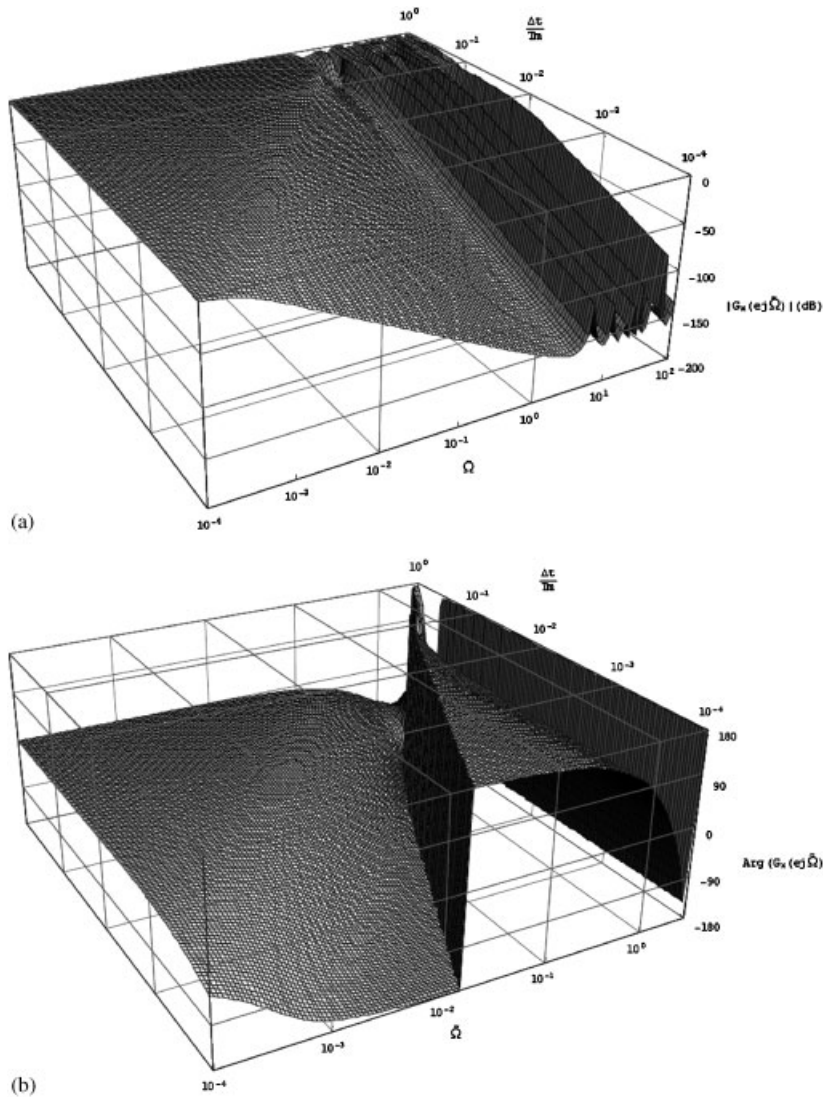
Figure 13. Error response for $\beta/4T_m = 10$, $T/T_m = 10$ and unit step input: (a) gain Bode plot; and (b) phase Bode plot.

one can see from Figure 13(b), that the MCS algorithm is out-of-phase with the forcing term for large values of $\tilde{\Omega}$.

6. REPRESENTATIVE NUMERICAL SIMULATIONS AND TESTS

In order to highlight the performances of the MCS algorithm and confirm the analytical findings of the previous sections, numerical simulations provided by means of the discrete

implementation of the MCS algorithm in SIMULINK [31] was performed. Moreover, some simulations will include a high-frequency noise will be described in order to confirm the validity of frequency-domain analyses. A first-order plant is emulated through a numerical or an electronic lag characterized by the following transfer function:

$$G[s] = \frac{1}{1 + Ts} \tag{64}$$

where T is the plant time constant. In order to perform experimental tests, the DS1104 R&D Controller board was used [32].

6.1. Numerical simulations

The simulations presented herein intend to validate some of analytical findings presented in Section 4.2. In fact, by means of the SG space depicted in Figure 3, it is possible to make a preliminary selection of the adaptive weight parameters β and α. Assuming the value $\Delta t / T_m = 0.1$ for accuracy reasons [29, p. 449], the ratio $\beta/\alpha = 0.1$ as proposed by Stoten [9] and a plant time constant $T/T_m = 1$, from the SG domain of Figure 3 we can choose a stable parameter $\beta/(4T_m) = 2$. From the same plot we can note that the assumption of $\beta/(4T_m) = 4$ will lead to system instability. The numerical simulations of this system, assuming a reference model time constant $T_m = 0.25$ s with the two different values of $\beta/(4T_m)$ is depicted in Figure 14. The system instability with $\beta/(4T_m) = 4$ is evident.

With the same reasoning, the parameter selection through the GS domain of Figure 4 is introduced. Assuming the value $\Delta t / T_m = 0.1$, $\beta/(4T_m) = 25$ and a plant time constant $T = 10T_m$, from the GS domain of Figure 4 we can choose a stable ratio $\beta/(\alpha 4T_m) = 0.1$ with $t_s = 4T_m = 1$ s; the same value is suggested by Stoten [9]. From the same plot we can note that the assumption of $\beta/(\alpha 4T_m) = 0.01$ will lead to system instability. As confirmation of these findings, the numerical simulations of this system, with reference model time constant $T_m = 0.25$ s, with the two different β/α ratios is depicted in Figure 15. Even in this case, the system instability with $\beta/\alpha = 0.01$ is quite evident.

The effect of a high-frequency noise applied to the feedback loop of the controller is analysed herein, by means of some numerical simulations and the frequency-domain analysis proposed in Section 5. The evolution of a MCS controlled system is depicted in Figure 16 assuming the value $\Delta t / T_m = 0.02$, $\beta/T_m = 1$, $T_m = 0.25$ s, $\beta/\alpha = 0.1$ and plant time constant $T = 2.5$ s. The system response depicted in Figure 16(a) is affected by a noise in the feedback loop with a circular frequency 232.4 rad/s; while the system response represented in Figure 16(b) is characterized by a noise with a circular frequency of 20.1 rad/s. The second system presents oscillations in the transient and in the steady-state regimes more marked than those of the first system. This can be deduced also from the analysis of the gain Bode plot of Figure 11, where the gain $G_x[e^{j\tilde{\omega}\Delta t}]$ of the system with $\tilde{\omega} = 20.1$ rad/s ($\tilde{\Omega} = 0.1$) and $\Delta t / T_m = 0.02$ is higher than the system with $\tilde{\omega} = 232.4$ rad/s ($\tilde{\Omega} = 1.16$) and $\Delta t / T_m = 0.02$. For these reasons we confirm the capacity of the MCS algorithm with the ZOH sampling to damp out high frequency forcing components.

Figures 17(a) and (b) show the response of the controlled system when $\Delta t / T_m = 0.4$ and $\Delta t / T_m = 0.04$, respectively, $\beta/(4 T_m) = 1$, $T/T_m = 1$ and the unit step input are assumed. One may observe that the error x_e is reduced for the case $\Delta t / T_m = 0.04$. This is confirmed from the values depicted in Figure 6(a) which shows an increase of numerical damping $\bar{\xi}$ for this particular condition. Moreover, one can clearly observe from Figure 17(b) that the damping
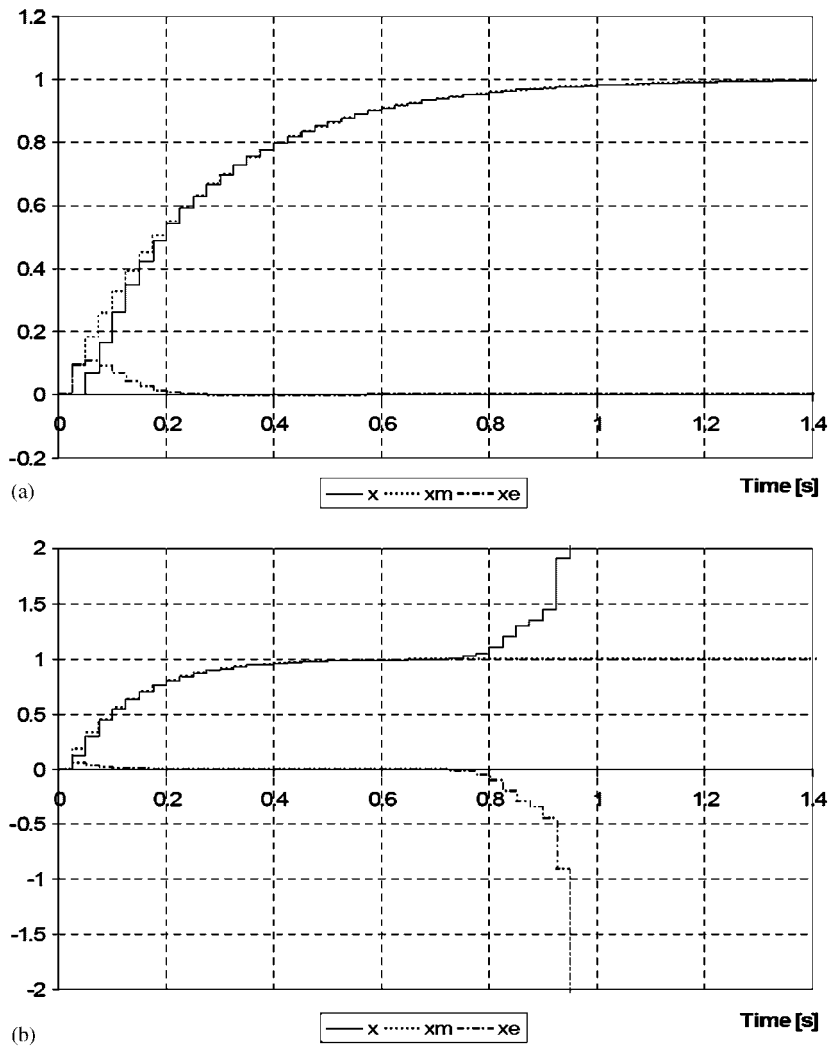
Figure 14. Evolution of the MCS controlled system for $T/T_m = 1$, $\Delta t/T_m = 0.1$, $\beta/(\alpha 4T_m) = 0.1$ and a unit step input: (a) $\beta/(4T_m) = 2$; and (b) $\beta/(4T_m) = 4$.

effect which reduces the tracking error is generated by the negative value of the feedback gain K in (30).

6.2. Tests

The experimental tests presented here intend to show the limited capability of the MCS algorithm with the ZOH sampling to deal with unresolved high frequencies without any specific device or filter. In fact, we have seen from Figures 13 and 16, the limited capability of the MCS
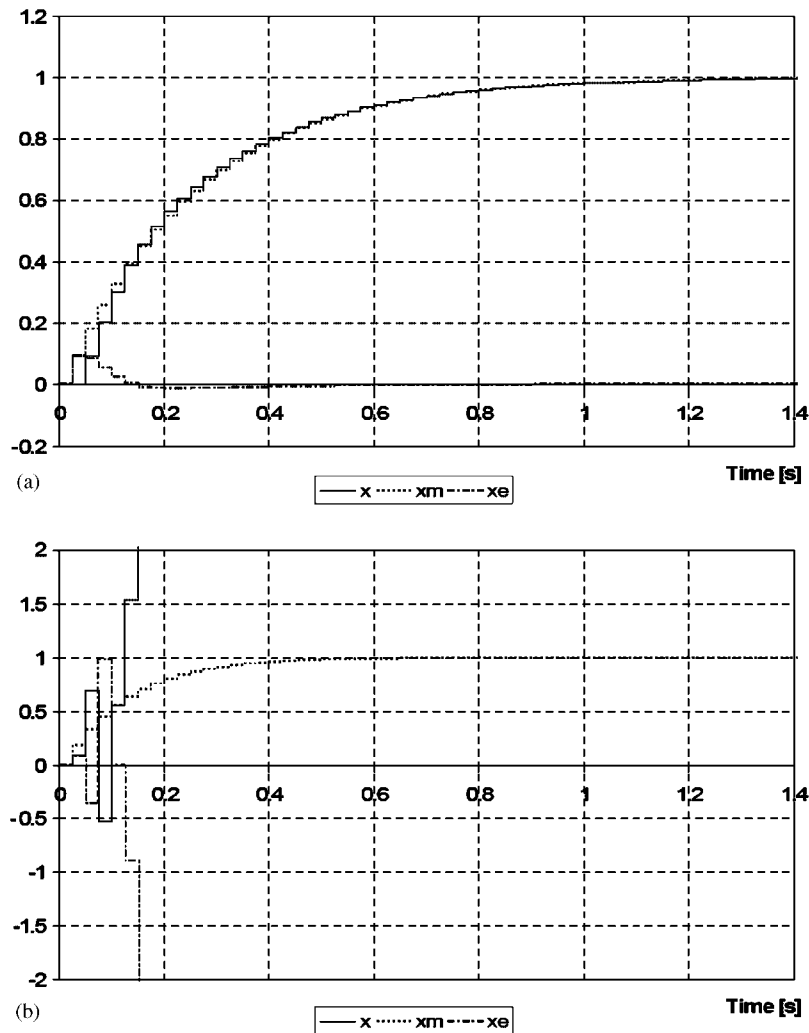
Figure 15. Evolution of the MCS controlled system for $T/T_m = 10$, $\Delta t/T_m = 0.1$, $\beta/(4T_m) = 25$ and unit step input: (a) $\beta/\alpha = 0.1$; and (b) $\beta/\alpha = 0.01$.

algorithm to damp out high frequencies for high $\Delta t/T_m$ ratios. In this respect, we considered a system with the following parameters: $\Delta t/T_m = 0.5$, $\beta/(4T_m) = 10$, $T/T_m = 9.98$, step input $r[k] = 0.1$ and $\beta/(\alpha 4T_m) = 0.1$. The relevant results depicted in Figure 18(a) show a favourable response of the system, even if it is sampled at the Nyquist frequency. The next simulation is conducted with $\beta/(4T_m) = 100$ and all other parameters unvaried. The corresponding results are depicted in Figure 18(b) and show a blow-up of the system due to unresolved frequencies. Note that the corresponding simulation conducted in a numerical environment, without disturbances, does not exhibit any problem.
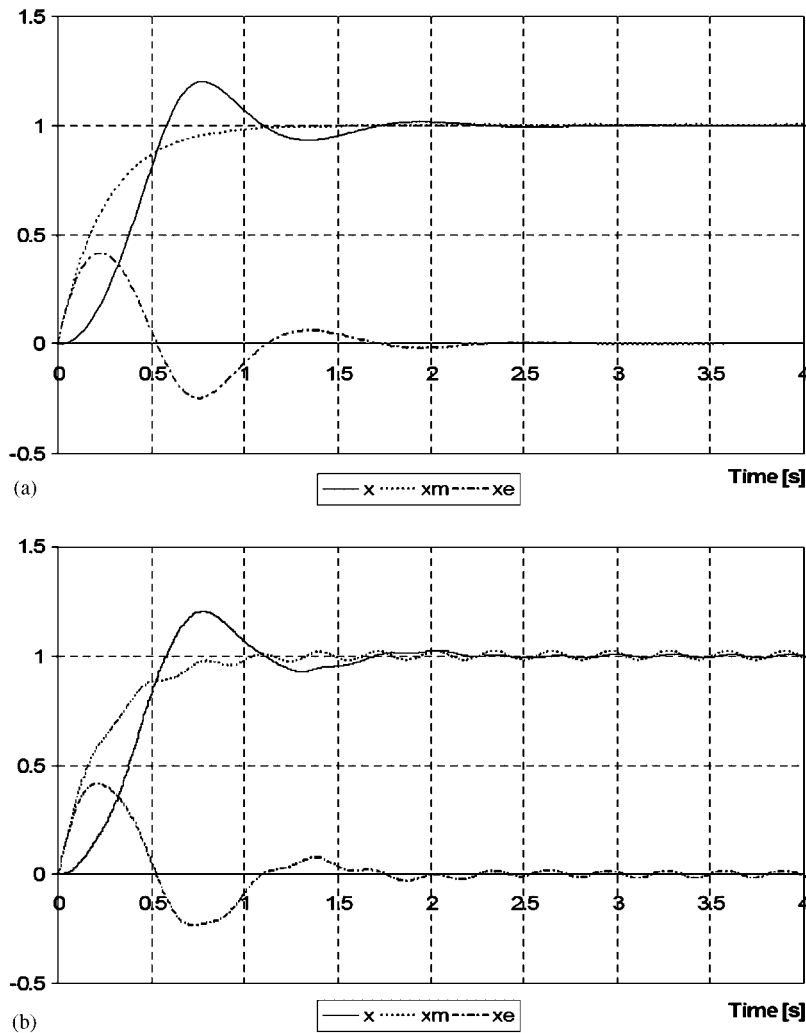
Figure 16. Evolution of the MCS controlled system for $T/T_m = 10$, $\Delta t/T_m = 0.02$, $\beta/(4T_m) = 1$, $\alpha/\beta = 10$ and unit step input: (a) high-frequency noise $\tilde{\omega} = 232.4$ rad/s; high-frequency noise $\tilde{\omega} = 20.1$ rad/s.

7. CONCLUSIONS AND PERSPECTIVES

This paper has dealt with the convergence and steady-state analysis of a discrete first-order MCS controller discretized with the one-step one-stage ZOH sampling. It was assumed that the plant to be controlled is a first-order system and the communication between plant and controller is zero-order sampled. The control signal is generated from the demand and the feedback from the plant instantaneously, thus resulting in no computational delay. The analysis performed here is for the case where the demand is a unit step input or fractions of it.

This analysis allowed two gain space domains to be determined in order to define the region of local stability. Moreover, the accuracy analysis has provided insight into the range of
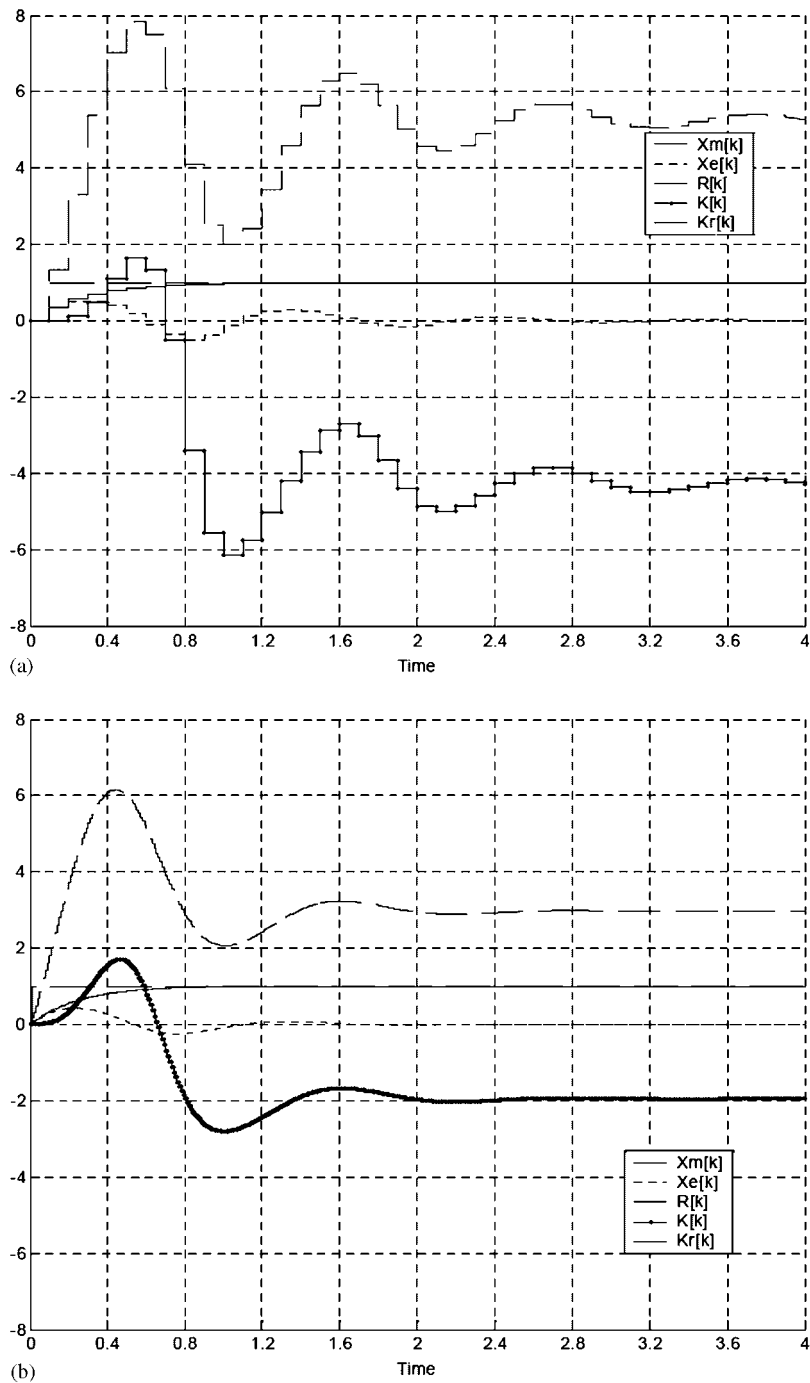
Figure 17. Evolution of the MCS controlled system for $\beta/(4T_m) = 1$, $T/T_m = 10$ and unit step input: (a) $\Delta t/T_m = 0.4$; and (b) $\Delta t/T_m = 0.04$.
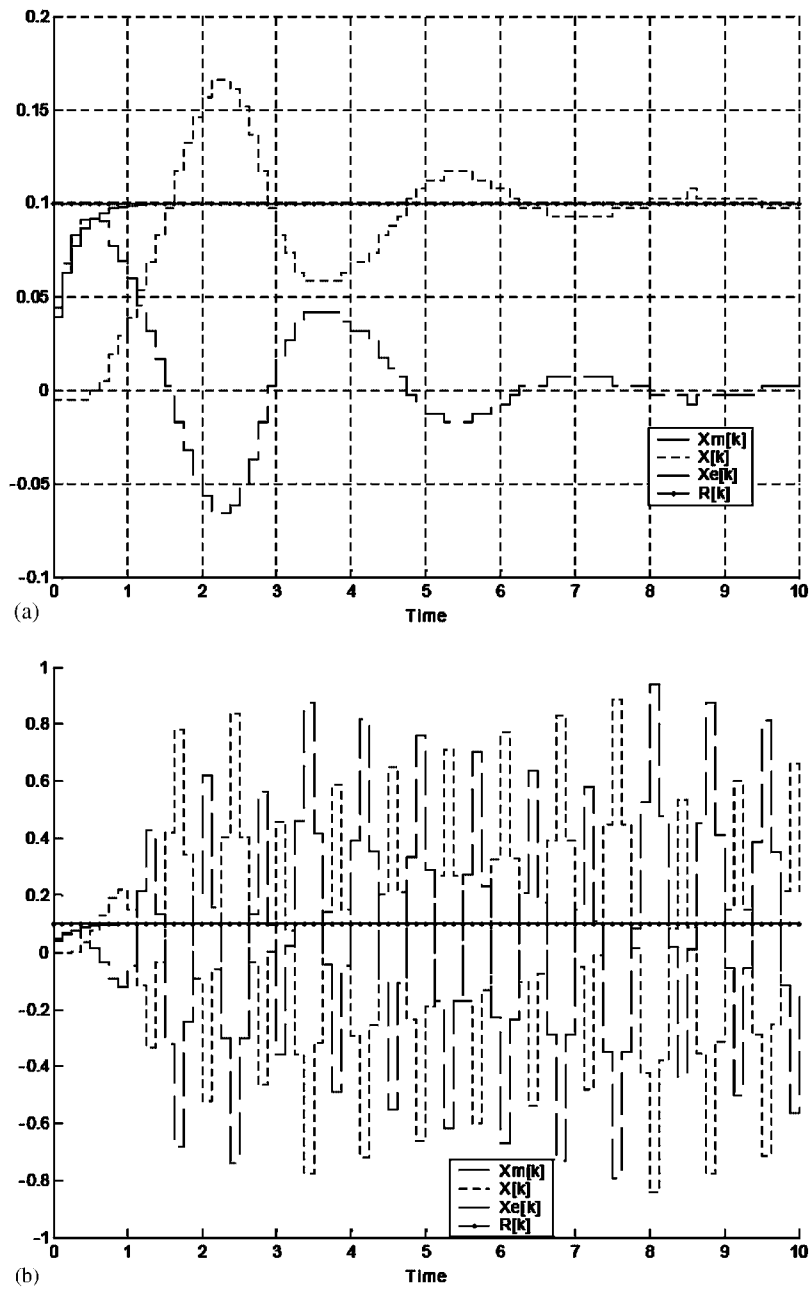
Figure 18. Evolution of the MCS algorithm with the DS1104 R&D Controller Board for $T/T_m = 9.98$, $\Delta t/T_m = 0.5$, step input $r[k] = 0.1$ and $\beta/(\alpha 4 T_m) = 0.1$: (a) $\beta/(4T_m) = 10$; and (b) $\beta/(4T_m) = 100$.

adaptive control weightings that results in optimal performance of the MCS controller and also highlights a possible approach to *a priori* selection of the time step and adaptive weighting values. Moreover, the frequency-domain analysis has shown the limited capability of the MCS algorithm with the ZOH sampling to filter out high frequencies for large values of the sampling interval or small time constants of the reference model. Numerical simulations and experimental tests confirm the main analysis conclusions, also in presence of noise and disturbance.

Further, the analyses were performed assuming no computational delay and the introduction of a full-sample period delay, which represents the worst case, should be investigated. Finally the analysis suggested in this paper should be performed on the error-based version of the MCS algorithm with integral action [9] considering more general inputs.

APPENDIX A

A.1. Amplification matrix

Matrices $\mathbf{A}_{IT}$, $\mathbf{B}_{IT}$ and vector $\mathbf{g}$ read

$$\mathbf{A}_{IT} = \begin{bmatrix} A'_m - B'\beta C_e(x[k]^2 + r[k]^2) & A'_m - A' & -B'x[k] & -B'r[k] \\ B'\beta C_e(x[k]^2 + r[k]^2) & A' & B'x[k] & B'r[k] \\ \beta x[k]C_e & 0 & 1 & 0 \\ \beta r[k]C_e & 0 & 0 & 1 \end{bmatrix} \tag{A1}$$

$$\mathbf{B}_{IT} = \begin{bmatrix} B'\sigma C_e(r[k-1]r[k] + x[k-1]x[k]) & 0 & 0 & 0 \\ -B'\sigma C_e(r[k-1]r[k] + x[k-1]x[k]) & 0 & 0 & 0 \\ -\sigma x[k-1]C_e & 0 & 0 & 0 \\ -\sigma r[k-1]C_e & 0 & 0 & 0 \end{bmatrix} \tag{A2}$$

$$\mathbf{g} = \begin{Bmatrix} B'_m r[k] \\ 0 \\ 0 \\ 0 \end{Bmatrix} \tag{A3}$$

Moreover, the amplification matrix $\mathbf{C}_{IT}$ reads

$$\mathbf{C}_{IT} = \begin{bmatrix} A'_m - B'\beta C_e(x[k]^2 + r[k]^2) & B'\sigma C_e(r[k-1]r[k] + x[k-1]x[k]) & A'_m - A' & -B'x[k] & -B'r[k] \\ 1 & 0 & 0 & 0 & 0 \\ B'\beta C_e(x[k]^2 + r[k]^2) & -B'\sigma C_e(r[k-1]r[k] + x[k-1]x[k]) & A' & B'x[k] & B'r[k] \\ \beta x[k]C_e & -\sigma x[k-1]C_e & 0 & 1 & 0 \\ \beta r[k]C_e & -\sigma r[k-1]C_e & 0 & 0 & 1 \end{bmatrix} \tag{A4}$$

A.2. External stability and eigenvalue bounds

In this subsection, we prove the external stability of (42). In detail, the stability of the overall system can be proved as follows:

$$\|\mathbf{y}[k+1]\|_2 = \left\|\boldsymbol{\Phi}\boldsymbol{\Lambda}^{k+1}\boldsymbol{\Phi}^{-1}\mathbf{y}[0] + \sum_{j=0}^{k}\boldsymbol{\Phi}\boldsymbol{\Lambda}^{k-j}\mathbf{c}_f 1^j\right\|_2 \leqslant \left\|\boldsymbol{\Phi}\boldsymbol{\Lambda}^{k+1}\boldsymbol{\Phi}^{-1}\mathbf{y}[0]\right\|_2 + \left\|\sum_{j=0}^{k}\boldsymbol{\Phi}\boldsymbol{\Lambda}^{k-j}\mathbf{c}_f 1^j\right\|_2$$

$$\leqslant \|\boldsymbol{\Phi}\|_2\left\|\boldsymbol{\Lambda}^{k+1}\right\|_2\left\|\boldsymbol{\Phi}^{-1}\mathbf{y}[0]\right\|_2 + \sum_{j=0}^{k}\|\boldsymbol{\Phi}\|_2\left\|\boldsymbol{\Lambda}^{k-j}\right\|_2\left\|\mathbf{c}_f 1^j\right\|_2$$

$$\leqslant \|\boldsymbol{\Phi}\|_2\rho(\boldsymbol{\Lambda})^{k+1}\left\|\boldsymbol{\Phi}^{-1}\mathbf{y}[0]\right\|_2 + \sum_{j=0}^{k}\|\boldsymbol{\Phi}\|_2\rho(\boldsymbol{\Lambda})^{k-j}\left\|c_f 1^j\right\|_2$$

$$\leqslant \|\boldsymbol{\Phi}\|_2 1\left\|\boldsymbol{\Phi}^{-1}\mathbf{y}[0]\right\|_2 + \sum_{j=0}^{k}\|\boldsymbol{\Phi}\|_2 1\left\|\mathbf{c}_f 1^j\right\|_2 \tag{A5}$$

where the spectral norm of $\boldsymbol{\Lambda}$ reads $\|\boldsymbol{\Lambda}\|_2 = \sup(\|\boldsymbol{\Lambda}x\|)/|x|$, $x \neq 0$ and $\rho(\boldsymbol{\Lambda}) = \|\boldsymbol{\Lambda}\|_2$ when $\boldsymbol{\Lambda}$ is a 5×5 matrix.

The expressions of λ_s of $\mathbf{C}_{IT,ss}$ defined in (40) in terms of the non-dimensional parameters defined in Section 4.1 read,

$$\lambda_1 = 1$$
$$\lambda_2 = 0$$
$$\lambda_3 = e^{-\Delta t/T_m}$$

$$\lambda_4 = \frac{1}{2}\left(1 + e^{-\Delta t/T} - \frac{2\beta(1 - e^{-\Delta t/T})}{T_m} - \sqrt{\frac{8(\beta - \alpha\Delta t)(1 - e^{-\Delta t/T})}{T_m} - 4e^{-\Delta t/T} + \left(1 - \frac{2\beta}{T_m} + \frac{e^{-\Delta t/T}(2\beta + T_m)}{T_m}\right)^2}\right) \tag{A6}$$

$$\lambda_5 = \frac{1}{2}\left(1 + e^{-\Delta t/T} - \frac{2\beta(1 - e^{-\Delta t/T})}{T_m} + \sqrt{\frac{8(\beta - \alpha\Delta t)(1 - e^{-\Delta t/T})}{T_m} - 4e^{-\Delta t/T} + \left(1 - \frac{2\beta}{T_m} + \frac{e^{-\Delta t/T}(2\beta + T_m)}{T_m}\right)^2}\right)$$

Finally, the lower and upper bound of $\beta/(4T_m)$ which entail complex conjugates values for λ_4 and λ_5 are reported below

$$\frac{\beta^{\mathrm{L}}}{4T_m} = \frac{1 - e^{\Delta t/T} + 2(\alpha\Delta t/\beta)e^{\Delta t/T} - 2\sqrt{(\alpha\Delta t/\beta)e^{\Delta t/T}\left(1 - e^{\Delta t/T} + (\alpha\Delta t/\beta)e^{\Delta t/T}\right)}}{8(e^{\Delta t/T} - 1)}$$

$$\frac{\beta^{\mathrm{U}}}{4T_m} = \frac{1 - e^{\Delta t/T} + 2(\alpha\Delta t/\beta)e^{\Delta t/T} + 2\sqrt{(\alpha\Delta t/\beta)e^{\Delta t/T}\left(1 - e^{\Delta t/T} + (\alpha\Delta t/\beta)e^{\Delta t/T}\right)}}{8(e^{\Delta t/T} - 1)} \tag{A7}$$

CONVERGENCE AND FREQUENCY ANALYSIS OF A DISCRETE CONTROLLER

REFERENCES

1. Åström KJ, Wittenmark B. *Adaptive Control*. Addison-Wesley Publishing Company: New York, 1995.
2. Sastry S. *Nonlinear Systems, Analysis, Stability and Control*. Springer: Berlin, 1999.
3. Wagg DJ. Adaptive control of nonlinear dynamical systems using a model reference approach. *Meccanica* 2003; **38**(2):227–238.
4. Kaufman H, Bar-Kana I, Sobel K. *Direct Adaptive Control Algorithms: Theory and Applications*. Springer: New York, 1994.
5. Housner GW, Bergman LA, Caughey TK, Chassiakos AG, Claus RO, Masri SF, Skelton RE, Soong TT, Spencer Jr BF, Yao TP. Structural control: past, present, and future. *Journal of Engineering Mechanics* 1997; **123**(9):897–971.
6. Faravelli L, Rossi R. Adaptive fuzzy control: theory versus implementation. *Journal of Structural Control* 2002; **9**:59–73.
7. Stoten DP, Benchoubane H. Empirical studies of an MRAC algorithm with minimal controller synthesis. *International Journal of Control* 1990; **51**(4):823–849.
8. Stoten DP, Benchoubane H. Robustness of a minimal controller synthesis algorithm. *International Journal of Control* 1990; **51**(4):851–861.
9. Stoten DP, Neild SA. The error-based minimal control synthesis algorithm with integral action. *Proceeding Institutions of Mechanical Engineers—Part I* 2003; **217**:187–201.
10. Stoten DP, Di Bernardo M. Application of the minimal control synthesis algorithm to the control and synchronization of chaotic systems. *International Journal of Control* 1996; **65**(6):925–938.
11. Bonelli A, Bursi OS. Generalized-α methods for seismic structural testing. *Earthquake Engineering and Structural Dynamics* 2004; **33**:1067–1102.
12. Wagg DJ, Stoten DP. Substructuring of dynamical systems via the adaptive minimal control synthesis algorithm. *Earthquake Engineering and Structural Dynamics* 2001; **30**(6):865–877.
13. Neild SA, Stoten DP, Drury D, Wagg DJ. Control issues relating to real-time substructuring experiments using a shaking table. *Earthquake Engineering and Structural Dynamics* 2005; **34**:1171–1192.
14. Magonette G. Development and application of large-scale continuous pseudo-dynamic testing techniques. *Philosophical Transactions of the Royal Society: Mathematical, Physical and Engineering Sciences* 2001; **359**:1771–1799.
15. Chu SY, Soong TT, Lin CC, Chen YZ. Time-delay effect and compensation on direct output feedback controlled mass damper systems. *Earthquake Engineering and Structural Dynamics* 2002; **31**(1):121–137.
16. Shampine LF, Reichtel MW. The MATLAB ODE suite. *SIAM Journal on Scientific Computing* 1997; **18**(1):1–22.
17. Narendra KS, Lin YH. Stable discrete adaptive control. *IEEE Transaction of Automatic Control* 1980; **AC-25**:456–461.
18. Datta A. Robustness of discrete-time adaptive controllers: an input-output approach. *IEEE Transaction of Automatic Control* 1993; **38**(12):1852–1857.
19. Park KC, Belvin WK. Partitioned solution procedure for control-structure interaction simulations. *Journal of Guidance, Control and Dynamics* 1991; **14**(1):59–67.
20. Agranovich G, Ribakov Y, Blostotsky B. A method for fast simulation of seismically excited active controlled MDOF structures. *Structural Control and Health Monitoring* 2004; **11**(4):369–378.
21. Stoten DP. *Model Reference Adaptive Control of Manipulators*. Wiley: New York, 1990.
22. Landau YD. *Adaptive Control—The Model Reference Approach*. Marcel Dekker Inc.: New York, 1979.
23. Young DM. *Iterative Solutions of Large Linear Systems*. Academic Press: Orlando, 1971.
24. Dutton K, Thompson S, Barraclough B. *The Art of Control Engineering*. Addison Wesley: Longman, Harlow, England, 1997.
25. Vulcan L. Discrete-time analysis of integrator algorithms applied to S.I.S.O. adaptive controllers with minimal control synthesis. *Ph.D. Thesis*, Department of Mechanical and Structural Engineering, University of Trento, 2006.
26. Bacciotti A, Mazzi L. A necessary and sufficient condition for bounded-input bounded-state stability of nonlinear systems. *SIAM Journal of Control Optimization* 2000; **39**(2):478–491.
27. Yang L, Neild SA, Wagg DJ, Virden DW. Model reference adaptive control of a nonsmooth dynamical system. *Nonlinear Dynamics* 2005, accepted.
28. Chung J, Hulbert GM. A time integration algorithm for structural dynamics with improved numerical dissipation: the generalized-α method. *Journal of Applied Mechanics* 1993; **60**:371–375.
29. Franklin GF, Powell JD, Workman ML. *Digital Control of Dynamical Systems* (3rd edn). Addison-Wesley: U.S.A., 1998.
30. Mugan A. Frequency domain analysis of time-integration algorithms. *Computer Methods in Applied Mechanics and Engineering* 2001; **190**:5777–5793.
31. The Mathworks, *MATLAB & SIMULINK*, Ver. 6.5.1. The Mathworks, Inc.: Natick, MA, U.S.A., 2003.
32. dSPACE, *Real-Time Interface, Implementation Guide*, Release 4.0. dSPACE GmbH: Paderborn, Germany, 2003.